Published OnlineFirst April 11, 2017; DOI: 10.1158/0008-5472.CAN-17-0502

Integrated Systems and Technologies: *Mathematical Oncology*

Cancer Research

# An *Ex Vivo* Platform for the Prediction of Clinical Response in Multiple Myeloma

Ariosto Silva[1], Maria C. Silva[1], Praneeth Sudalagunta[1], Allison Distler[2], Timothy Jacobson[1], Aunshka Collins[2], Tuan Nguyen[2], Jinming Song[3], Dung-Tsa Chen[4], Lu Chen[4], Christopher Cubitt[5], Rachid Baz[2], Lia Perez[6], Dmitri Rebatchouk[7], William Dalton[8], James Greene[9], Robert Gatenby[10], Robert Gillies[1], Eduardo Sontag[9], Mark B. Meads[2,11], and Kenneth H. Shain[2,11]

## Abstract

Multiple myeloma remains treatable but incurable. Despite a growing armamentarium of effective agents, choice of therapy, especially in relapse, still relies almost exclusively on clinical acumen. We have developed a system, *Ex vivo* Mathematical Myeloma Advisor (EMMA), consisting of patient-specific mathematical models parameterized by an *ex vivo* assay that reverse engineers the intensity and heterogeneity of chemosensitivity of primary cells from multiple myeloma patients, allowing us to predict clinical response to up to 31 drugs within 5 days after bone marrow biopsy. From a cohort of 52 multiple myeloma patients, EMMA correctly classified 96% as responders/nonresponders and correctly classified 79% according to International Myeloma Working Group stratification of level of response. We also observed a significant correlation between predicted and actual tumor burden measurements (Pearson $r = 0.5658$, $P < 0.0001$). Preliminary estimates indicate that, among the patients enrolled in this study, 60% were treated with at least one ineffective agent from their therapy combination regimen, whereas 30% would have responded better if treated with another available drug or combination. Two *in silico* clinical trials with experimental agents ricolinostat and venetoclax, in a cohort of 19 multiple myeloma patient samples, yielded consistent results with recent phase I/II trials, suggesting that EMMA is a feasible platform for estimating clinical efficacy of drugs and inclusion criteria screening. This unique platform, specifically designed to predict therapeutic response in multiple myeloma patients within a clinically actionable time frame, has shown high predictive accuracy in patients treated with combinations of different classes of drugs. The accuracy, reproducibility, short turnaround time, and high-throughput potential of this platform demonstrate EMMA's promise as a decision support system for therapeutic management of multiple myeloma. *Cancer Res; 77(12); 1–16. ©2017 AACR.*

## Major Findings

We have developed a novel tool capable of predicting, within 5 days, 3 month clinical response of multiple myeloma patients to 31 drugs, using fresh bone marrow aspirates, a digital image analysis algorithm, mathematical models, and pharmacokinetic data.

## Introduction

For decades, there have been attempts to develop predictive biomarkers in cancer, unfortunately, with limited translational success (1). Most biomarker development today depends on molecular techniques applied to dead cells, cell lines, or primary cancer cells isolated from their microenvironment, thus failing to account for many elements needed to properly assess therapeutic efficacy (2). We anticipate that the development of novel technologies and multidisciplinary approaches to directly assess chemosensitivity of primary cells in *ex vivo* reconstructions of the tumor microenvironment (TME) are critical avenues toward personalized predictive biomarker development (3–5).

Multiple myeloma is a treatable, but incurable malignancy of plasma cells (6), which serves as an excellent model disease to examine the potential of personalized management strategies. Frontline therapy combining multiple novel agents, high-dose therapy with autologous stem cell transplant, and maintenance therapy has yielded a high success rate of response in multiple myeloma (7). However, all patients eventually relapse, with the treatment of relapsed patients relying mainly on clinical acumen. This empirical approach has been made increasingly more difficult by the large number of approved anti–multiple myeloma agents, leading to astronomical numbers of possible two-, three-, or even four-drug combinations. In addition, at least one or two cycles of therapy are required to determine clinical efficacy, during which time the patient may suffer side effects without clinical

[1]Department of Cancer Imaging and Metabolism, H. Lee Moffitt Cancer Center and Research Institute, Tampa, Florida. [2]Department of Malignant Hematology, H. Lee Moffitt Cancer Center and Research Institute, Tampa, Florida. [3]Department of Hematologic Pathology, H. Lee Moffitt Cancer Center and Research Institute, Tampa, Florida. [4]Department of Statistics, H. Lee Moffitt Cancer Center and Research Institute, Tampa, Florida. [5]Translational Medicine Core, H. Lee Moffitt Cancer Center and Research Institute, Tampa, Florida. [6]Department of Bone Marrow Transplantation, H. Lee Moffitt Cancer Center and Research Institute, Tampa, Florida. [7]nPharmakon, LLC, Piscataway, New Jersey. [8]M2Gen, Tampa, Florida. [9]Rutgers, New Brunswick, NJ. [10]Department of Radiology, H. Lee Moffitt Cancer Center and Research Institute, Tampa, Florida. [11]Department of Tumor Biology, H. Lee Moffitt Cancer Center and Research Institute, Tampa, Florida.

**Note:** Supplementary data for this article are available at Cancer Research Online (http://cancerres.aacrjournals.org/).

**Corresponding Author:** Kenneth H. Shain, H. Lee Moffitt Cancer Center and Research Institute, 12902 Magnolia Dr., SRB2, Tampa, FL 33612. Phone: 813-745-4748; Fax: 813-745-6817; E-mail: ken.shain@moffitt.org

**doi:** 10.1158/0008-5472.CAN-17-0502

Published OnlineFirst April 11, 2017; DOI: 10.1158/0008-5472.CAN-17-0502



## Quick Guide to Equations and Assumptions

We have implemented a gray-box parametric model that represents the tumor's response to drugs as a collective of subpopulations, each with different levels of chemosensitivity. In this model, the likelihood of cell death depends on drug concentration and exposure time. This model is parameterized by an *ex vivo* chemosensitivity assay, where primary multiple myeloma cells from fresh bone marrow aspirates are exposed to different concentrations of drug for 96 hours (Fig. 1; Supplementary Fig. S1).

Suppose the population of multiple myeloma cells in the patient's body is represented by $p(t)$. The tumor burden varies with time according to the difference equation:

$$p(t+dt) = p(t) \times G(dt) \times D(t,dt), \quad G(dt) = \left(1 + \mathrm{LI}\left(2^{\Delta t} - 1\right)\right)^{dt/\Delta t}, \tag{A}$$

where $G(dt)$ represents growth due to tumor cell replication and $D(t,dt)$ represents drug-induced cell death between times $t$ and $t+dt$. In cell culture, doubling time is used as a metric for quantifying cell replication. For mammalian cells, this number is approximately 24 hours. However, the doubling time of multiple myeloma tumors is much longer due to its characteristically low proliferative index (*LI*, labeling index). In the mathematical model, the growth factor for the multiple myeloma population in the absence of therapy is given by Equation A, where $dt$ is a time interval (in days), and $\Delta t$ is the time step used in the simulation's calculation. To determine *LI* for a given patient, we use the two closest prebiopsy measures of tumor burden, obtained from monoclonal paraprotein, and Equation A, with $D = 1$.

To describe the stochastic cell death process, we propose an empirical pharmacodynamics model based on the drug occupancy theory (8):

$$[\mathrm{Drug}] + [\mathrm{Receptor}] \underset{\text{Dissociation}}{\overset{\text{Binding}}{\rightleftharpoons}} \begin{bmatrix}\text{Drug-Receptor}\\ \text{Complex}\end{bmatrix} \xrightarrow{\text{Threshold}} \text{Cell death}, \frac{d\beta}{dt} = \underbrace{-\kappa\beta(t)}_{\text{Dissociation}} + \underbrace{R(t)^h}_{\text{Binding}}, \tag{B}$$

where drug and receptor molecules form drug–receptor complexes, which in turn cause cellular damage $\beta$ and, eventually, cell death. The dynamics of this reversible reaction follow the law of mass action (9), where $R(t)$ is the drug concentration at time $t$, $h$ is an empirical exponent denoting the rate of conversion of drug exposure into cell damage, and $\kappa$ of cell damage repair.

When the cellular damage is greater than the threshold $\tau$, the probability of cell death increases asymptotically:

$$D(t,dt) = 1 - 0.5 \times \tanh(\alpha(t)/2) \times dt, \alpha(t,dt) = \max\left(\frac{\beta(t,dt) - \tau}{\delta}, 0\right), \tag{C}$$

where $\delta$ is a nondimensionalizing empirical factor.

Short-term response of multiple myeloma patients to therapy can be monotonic or present an inflexion point followed by relapse (Fig. 2A–C). Thus, tumor chemosensitivity cannot always be accurately described by a single "clonal" population, but requires a more nuanced representation in the general model. We propose two subpopulations, with different degrees of sensitivity to therapy. Each subpopulation can either be modeled as "clonal" or as a distribution, with drug-specific threshold values ($\tau$, Equation D). These threshold values are obtained from a normally distributed probability density function that specifies the fraction of a subpopulation that initiates cell death beyond a given threshold. Figure 2B shows an example of such a representation of tumor chemosensitivity as a single and as a double distribution. Thus, the total tumor burden of a patient is represented as:

$$p(t+dt) = \sum p_{j,i}(t) \times G(dt) \times D_j(t,dt,\tau_i), \quad j = 1,2 \text{ subpoplations. } i = 1,\ldots,n \text{ bins.}, \tag{D}$$

where the composition of each subpopulation at initial time $t_0$ is modeled as a distribution with a mean $\mu_j$ and standard deviation $\sigma_j$ that define the percentage of cells that initiate cell death when the accumulated damage surpasses $\tau$. For computational purposes, we have discretized this distribution in a histogram with $n$ bins, ranging from $\mu_j - 6\sigma_j$ to $\mu_j + 6\sigma_j$, using MATLAB's function *normpdf* (Supplementary Fig. S2).

There is no biological meaning for negative $\tau$, so the histogram is truncated when $\mu_j - 6\sigma_j < 0$, and the value of each bin is normalized so that the sum of all bins corresponds to $p_j$. Thus, at initial time $t_0$, the composition of the $j^{\text{th}}$ subpopulation is:

$$p_{j,i}(t_0) \approx \frac{\hat{p}_{j,i}(t_0)}{\sum_{i=1}^{n} \hat{p}_{j,i}(t_0)} \times p_j(t_0), \hat{p}_{j,i}(t_0) = \begin{cases} PDF\left(\tau_i; \mu_j, \sigma_j\right), & \forall \tau_i \geq 0 \\ 0, & \forall \tau_i < 0. \end{cases} \tag{E}$$

To separate drug-induced and spontaneous cell death, we divide every *ex vivo* dose-response curve by the corresponding vehicle control. Thus, the *ex vivo* data used to parameterize the mathematical model consist of percent live cells normalized by control at every time point, drug concentration, and exposure time. We then use MATLAB's *lsqcurvefit* function to find the model parameters that minimize the difference between normalized *ex vivo* data and the model estimates.

The last step consists of choosing among the four possibilities (1 or 2 subpopulations, clonal or distribution) the model that best describes the *ex vivo* data. We achieve this by applying Akaike's Information Criterion (AIC; ref. 10), which favors the best fitting model with the least number of parameters. Our simulations have shown that models with three or more subpopulations are never chosen, as they produce minor improvements in *ex vivo* data fitting, and are significantly penalized by AIC due to their large number of parameters (e.g., 1-population distribution requires 5 parameters, 2-subpopulation distributions require 9 parameters, 3-subpopulation distributions require 13 parameters).

In summary, the model assumes the existence of one or two tumor subpopulations, with different degrees of chemosensitivity. Each subpopulation, in turn, exhibits a range of sensitivity to therapy modeled as a normally distributed probability density function.

Published OnlineFirst April 11, 2017; DOI: 10.1158/0008-5472.CAN-17-0502



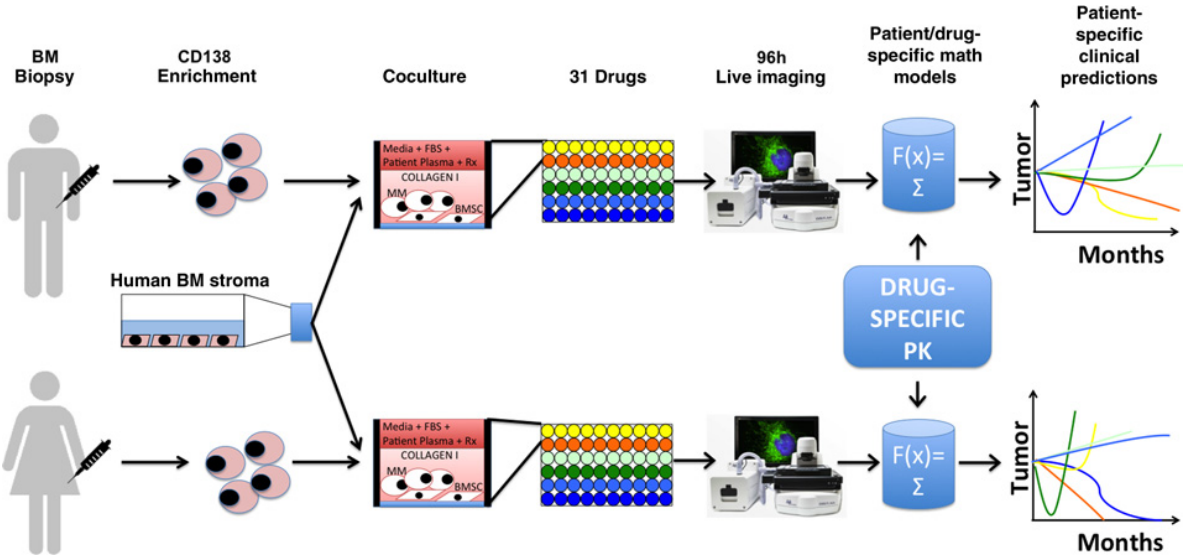


**Figure 1.**

A high-throughput *ex vivo* assay for prediction of clinical response in multiple myeloma. During a standard-of-care bone marrow biopsy, an extra volume of 10 mL aspirate is harvested in a heparin-coated tube. Multiple myeloma cells are obtained by selection for CD138 expression, and cocultured with previously established human bone marrow stroma (bone marrow mesenchymal stem cells, BMSC) and collagen in 384- or 1,536-multi well plates. The culture medium in each well is supplemented with the patient's own plasma, and the plate is incubated overnight for stroma adhesion and equilibration of soluble factors. The next day, the plate is drugged (up to 31 drugs in a 384- and 127 drugs in a 1,536-well plate) and placed in a microscope for bright-field live imaging for 4 days (1 picture every 30 minutes). A digital image analysis algorithm quantifies cell death (Fig. 2 and Supplementary Fig. S1) and generates *ex vivo* dose-response curves, which in turn are used to parameterize patient/drug-specific mathematical models of chemosensitivity. Each mathematical model is unique for a patient/drug combination. Once we include the drug-specific pharmacokinetic properties, available from phase I studies, to the patient/drug-specific mathematical models, EMMA creates 3-month predictions of clinical response. By comparing the predicted response of multiple drugs tested, it is possible to choose the best therapy for each patient. In the example above, the first patient would mostly benefit from treatment combining the "yellow" and "orange" drugs, whereas the best therapy for the second patient would include the "orange" and "blue" drugs. Importantly, these predictions are available 5 days after biopsy, and thus could be incorporated in the clinical decision-making process.

benefit. Moreover, individual patients may be sensitive to targeted agents not formally investigated in multiple myeloma (11, 12). Thus, an assay capable of choosing the drug combination with highest clinical benefit would provide a critical step forward in the personalized treatment of relapsed multiple myeloma and other hematologic malignancies (13).

We describe an approach to predict clinical response of multiple myeloma patients to several classes of drugs, hereon referred to as *Ex vivo* Mathematical Myeloma Advisor (EMMA), designed to overcome the main hurdles that have limited the success of past and present technologies for assessment of clinical efficacy of experimental drugs in multiple myeloma. Historic colony formation assays require 2 to 3 weeks to yield results, which is beyond clinically actionable time. In addition, multiple myeloma cells have a low success rate of colony formation (1). Patient-derived tumor xenografts (PDX) models, although an invaluable tool for basic and translational research, are equally limited as predictive biomarkers due to extensive interval required for tumor engraftment and treatment response (14). Further, the infrastructure, financial burden, number of multiple myeloma cells, and, until recently, the lack of an appropriate host make PDX models suboptimal as clinically predictive biomarkers for testing the large number of drugs available in multiple myeloma (15). In contrast, using off-the-shelf multi-well plates, EMMA can test 31 drugs or combinations in 384-well plates, or 127 drugs in 1,536-well plates (16), with as few as 0.5 million multiple myeloma cells, thus allowing the clinical screening of an individual multiple myeloma patient to all standard-of-care and clinically relevant "non-multiple myeloma" therapeutics, in a single experiment.

In order to evaluate the accuracy of EMMA as a predictive multiple myeloma biomarker, we have tested samples of primary multiple myeloma cells from fresh bone marrow biopsies against multiple standard-of-care and experimental agents generating patient- and drug-specific mathematical models of chemosensitivity and clinical response to therapy within 5 days of biopsy. Crucially, we prospectively validated these *in silico* responses with postbiopsy treatment outcomes. EMMA also provides a platform to conduct *in silico* clinical trials to assess the efficacy of novel therapeutics. We assessed the efficacy of a series of experimental agents, including 25 protein kinases inhibitors (PKI), demonstrating patient-specific responses. Further, test/re-test reproducibility was demonstrated in patients with sequential biopsies. Collectively, these results support the use of EMMA as a novel rapid, reproducible, and high-throughput, *ex vivo*–, and mathematically informed decision-support tool for patient-specific multiple myeloma therapy.

## Materials and Methods

### Primary cancer cells

We investigated the *ex vivo* response of cancer cells from multiple myeloma patients (newly diagnosed or relapsed).

Published OnlineFirst April 11, 2017; DOI: 10.1158/0008-5472.CAN-17-0502



Investigators obtained signed informed consent from all patients who were enrolled on the clinical trials MCC#14745, MCC#14690, and MCC#18608 conducted at the H. Lee Moffitt Cancer Center and Research Institute, as approved by the Institutional Review Board. To this end, patient samples were utilized in accordance with the Declaration of Helsinki, International Ethical Guidelines for Biomedical Research Involving Human Subjects (CIOMS), Belmont Report, and U.S. Common Rule. The medical records were de-identified, and only the following clinically relevant information was reviewed: (A) treatment administered (therapeutic agents, doses, and schedule) prior to biopsy; (B) cytogenetics; and (C) serum and urine electrophoresis results.

### Cell lines

MM1.S myeloma cells were obtained from ATCC in 2009 and are validated biannually (last, February 2017) by comparing short tandem repeat analysis with ATCC's genetic profile (Geneteca) and screening for mycoplasma contamination by PCR (Agilent Technologies). Cells are utilized for only 2 to 8 passages before renewal with validated cryostorage aliquots.

### Stromal cells

The non–CD138-selected cells from bone marrow aspirates were placed in a flask with RPMI 1640 media supplemented with FBS (heat inactivated), penicillin/streptomycin, and passaged until only adherent cells remained (17). As this process takes weeks, primary multiple myeloma cells from fresh biopsies were cocultured with established stroma from prior patient samples.

### *Ex vivo* assay

The *ex vivo* assay used to quantify chemosensitivity of primary multiple myeloma cells was described in detail previously (16). Briefly, fresh bone marrow aspirate cells are enriched for $CD138^+$ expression using magnetic beads. Multiple myeloma cells ($CD138^+$) were seeded in multi-well plates with collagen-I and previously established human-derived stroma, to a total volume of 8 μL containing approximately 4,000 multiple myeloma cells and 1,000 stromal cells. Each well is filled with 80 μL of RPMI 1640 media supplemented with FBS (heat inactivated), penicillin/streptomycin, and patient-derived plasma (10%, freshly obtained from patient's own aspirate, filtered) and left overnight for adhesion of stroma (Supplementary Figs. S1 and S3). The next day, drugs were added using a robotic plate handler, so that every drug was tested at five concentrations (1:3 serial dilution) in two replicates. Negative controls (supplemented growth media with and without vehicle control, DMSO) were included, as well as positive controls for each drug (cell line MM1.S at highest drug concentration). Plates were placed in a motorized stage microscope (EVOS Auto FL; Life Technologies) equipped with an incubator and maintained at 5% $CO_2$ and 37°C. Each well was imaged every 30 minutes for a total duration of 4 days (Supplementary Figs. S1, S3, and S4).

### Digital image analysis algorithm

We have developed a digital image analysis algorithm previously described (8, 16) to determine changes in viability of each well longitudinally across the 96-hour interval. In summary, this algorithm computes differences in sequential images and identifies as live cells those with continuous membrane deformations resulting from the interaction with the surrounding matrix. These interactions cease upon cell death. By applying this operation to all 192 images acquired for each well, it is possible to quantify nondestructively, and without the need to separate stroma and myeloma, the effect of drugs as a function of concentration and exposure time (Supplementary Fig. S1D and S1E).

### Simulation of clinical treatment

The ultimate goal of this work is to predict the clinical response of multiple myeloma patients to therapy using the proposed mathematical model of chemosensitivity, and the pharmacokinetic (PK) properties of the drug and regimen chosen. Below, we describe an example of prediction of treatment with carfilzomib, whose regimen consists of infusions on days 1, 2, 8, 9, 15, and 16 in a cycle of 28 days. Blood concentration of carfilzomib peaks at approximately 5.5 μmol/L upon injection, quickly decreasing to 30 nmol/L after 20′, 1.4 nmol/L at 1 hour, and 0.14 nmol/L after 4 hours (18).

To simulate the treatment of a patient, we replace the function $R(t)$ from Equation B by the PK curve of blood concentration of drug for the entire interval of the treatment. For example, let us consider patient Pt103, whose chemosensitivity to carfilzomib is depicted in Supplementary Fig. S5, drug concentrations ranged from 50 nmol/L to 0.6 nmol/L. Total exposure time was 96 hours, with imaging intervals of 30 minutes. Black dots represent actual data measurements. Green and blue surfaces represent distributed models of one and two populations, whereas cyan and red (overlapped) represent one and two population models with no distribution. As per the Akaike's Information Criterion (AIC), the two-population model with distribution is the best *ex vivo* fit.

The parameters for this patient's model of chemosensitivity to carfilzomib are listed in Supplementary Table S1. The *in vivo* growth rate, obtained from the rate of increase in monoclonal paraprotein from the latest relapse, is determined by the labeling index (*LI*) of 1.44%. Parameter $a_6$ indicates that there are two subpopulations within this tumor burden in terms of chemosensitivity to carfilzomib. The first, more sensitive, occupies 53% of the number of cells and the other, more resistant, 47%.

As mentioned earlier, the least squares method is used to estimate parameters for each of the four proposed models. The implementation of this method is done through MATLAB's *lsqcurvefit* function, which uses an iterative gradient-based optimization algorithm to find those parameter values that yield the smallest *SSR*. In order to determine how AIC's choice of the "best model" eliminates over-parameterization, we have conducted convergence studies on the parameters during *lsqcurvefit* optimization of patient Pt103's *ex vivo* response to panobinostat (see Supplementary Material).

Importantly, this approach does not require a training set: all parameter values are obtained by fitting a general set of equations to the *ex vivo* data, using AIC to penalize more complex and favor simpler models. Thus, this work is a type 4 TRIPOD study (19).

The following PK models were used for the patients tested in this study: bortezomib (20), carfilzomib (21), melphalan (22), liposomal doxorubicin (23), selinexor (CRM1i, investigator brochure), dexamethasone (24), lenalidomide (25), and pomalidomide (26).

### Generation of the heatmap representing the activity of 30 drugs in multiple myeloma cells from 13 patients

Twenty-five protein kinase inhibitors were tested in 13 primary multiple myeloma samples, at 10 μmol/L maximum concentration each (1:3 serial dilution, 5 concentrations, 2 replicates). We have

Published OnlineFirst April 11, 2017; DOI: 10.1158/0008-5472.CAN-17-0502



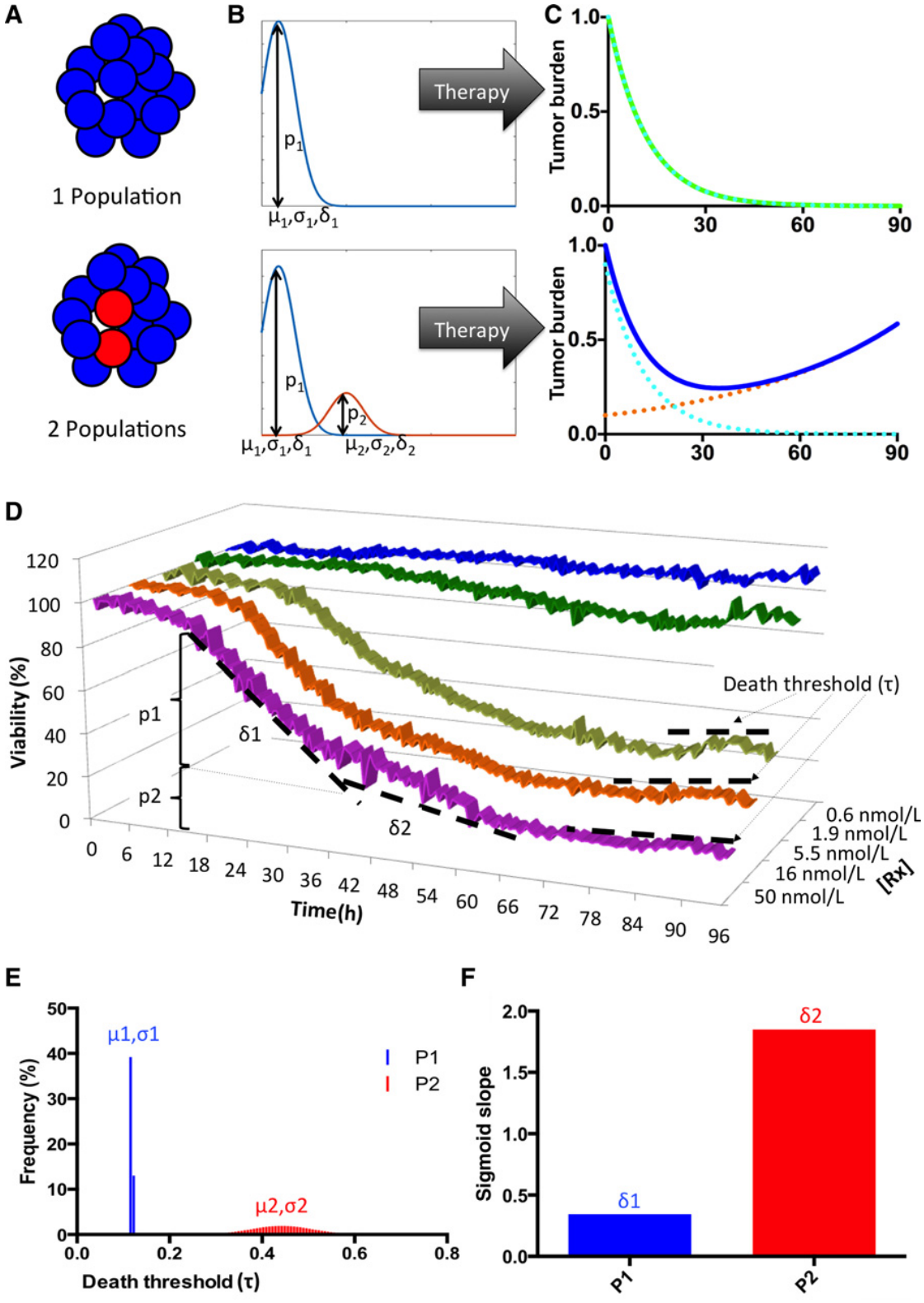

Published OnlineFirst April 11, 2017; DOI: 10.1158/0008-5472.CAN-17-0502



quantified the AUC (the average of viability between all replicates across 96 hours) of each drug for each patient sample and normalized this measure by the maximum possible AUC. If the drug showed no effect whatsoever, the normalized AUC would be 100%, whereas drugs with higher effect have a lower AUC. Drugs were sorted from most active (lowest average AUC) to least active (highest average AUC).

## Results

### *Ex vivo* data and mathematical models capture the heterogeneity of individual tumor chemosensitivity

Figure 1 and Supplementary Fig. S1 illustrate the workflow for *ex vivo* analysis of chemosensitivity: CD138-selected multiple myeloma cells obtained from fresh bone marrow aspirates were seeded in multi-well plates with collagen and previously established human-derived primary stroma. After overnight incubation to ensure stroma adhesion, 31 different drugs were added, and plates were imaged every 30 minutes for 4 days. As previously described (5, 16), a digital image analysis algorithm determined the number of viable cells in every well at each of the 192 time points, thus producing 1,920 data points per drug. Supplementary Fig. S1E demonstrates an output of the *ex vivo* assay. Curves represent changes in viability of primary multiple myeloma cells and a cell-line control to different drug concentrations during 96 hours. These data were used to parameterize patient-specific mathematical models of chemosensitivity (see Methods and Supplementary Material).

The central aspect of EMMA is the ability to characterize tumor heterogeneity in the form of subpopulations with different degrees of chemosensitivity to a given drug (Fig. 2A). The importance of proper characterization of tumor heterogeneity is depicted in Fig. 2B and C: a homogeneous tumor reacts to therapy monotonically, either by steadily decreasing viability (Fig. 2C, green line) or by sustained growth. A heterogeneous tumor, however, harboring a chemoresistant subpopulation, will have a curve of response characterized by an inflection point at the time of relapse (Fig. 2C, blue line). To identify these subpopulations from the *ex vivo* dose-response data, we test four hypotheses: the first assumes only one "clonal" population (all cells in the tumor have the same degree of sensitivity to one particular drug), the second assumes that there is one population, but its chemosensitivity follows a normal distribution. The two other models assume two "clonal" subpopulations or two distributions, respectively. EMMA identifies the parameters that best fit each of these four models to the *ex vivo* data (Fig. 2D) and chooses the best model after residue correction by AIC to avoid overfitting (10). In the example of Fig. 2E, EMMA's interpretation is that the tumor is composed of two subpopulations, $p_1$ and $p_2$: the first is more uniform ("clonal") and more sensitive, whereas the second has higher variance (Fig. 2E and F) and is more resistant.

### EMMA predicts clinical response of multiple myeloma patients to single agents or drug combinations

A total of 52 patient specimens were tested *ex vivo* against a panel of drugs, and EMMA model predictions were tested against clinical outcome to the same drugs. The median patient age was 64.5 years, 21 patients were female, 13 were newly diagnosed, and the majority relapsed and/or refractory (Table 1). In order to generate clinical predictions of response to therapy, EMMA simulates each of the drugs in a regimen independently and combines all responses assuming additivity. Figure 3 describes patient Pt111's response to a triplet regimen of carfilzomib (K), lenalidomide (R), and dexamethasone (D). Figure 3A depicts the *ex vivo* response to carfilzomib (black dots) as well as the mathematical model proposed by EMMA (blue surface). Figure 3B depicts the actual response of this patient to the three-agent treatment (black dots linked by dashed lines) and model-predicted response of this patient to carfilzomib as single agent (green line). Figure 3C–D and Fig. 3E–F represent *ex vivo* and clinical predictions for the same patient to dexamethasone and lenalidomide, respectively. The combination of the three models shows high correlation with the actual outcome (Fig. 3G). Figure 3H shows the predictions of clinical response for this patient to other drugs: those expected to be most clinically effective were carfilzomib, bortezomib, and liposomal doxorubicin, whereas pomalidomide and lenalidomide were predicted to have little effect on this patient's tumor.

***Classification of 52 multiple myeloma patients as responders or nonresponders.*** Clinically, multiple myeloma response is monitored over time via sequential measurements of serum or urine monoclonal antibody produced by malignant cells (paraprotein) as a surrogate assessment of tumor burden. The least strict level of validation for this predictive model was to classify patients as responders and nonresponders. Table 1 shows that this model correctly classified 50 of 52 patients (96%) according to response/no-response. The first exception, *Pt73* was predicted not to respond, but the cycle 2 day 1 paraprotein measure indicated a 70% tumor reduction. Unfortunately, this patient died 3 weeks later with disease progression, and no subsequent measures are available to confirm response/progression. *Pt95*'s model correctly predicted an initial response (Supplementary

**Figure 2.**

Mathematical representation of intratumoral heterogeneity of clinical response to a hypothetical treatment. **A,** Given any particular drug and a patient's tumor burden can be entirely sensitive to therapy (top), or contain a subpopulation of resistant cells (bottom). **B,** These subpopulations ($p_i$) can be characterized as mono- or bi-modal distributions, with corresponding thresholds for initiation of cell death determined by a mean ($\mu_i$) and standard deviation ($\sigma_i$), and a rate of drug-induced cell death ($\delta_i$). **C,** The clinical implication of this mathematical representation is that a homogeneous tumor will have a monotonic response to therapy, leading to a complete response, whereas a heterogeneous tumor will present an inflection point where the sensitive population is eradicated and the resistant cells promote tumor re-growth. **D,** In this example, we depict EMMA's analysis of the *ex vivo* response of patient Pt104's multiple myeloma cells to bortezomib in a 96-hour interval. There is a shift in the rate of cell death (from $\delta_1$ to $\delta_2$), more noticeable in the highest concentration (50 nmol/L, magenta) around 36 hours, indicating the depletion of the more sensitive subpopulation ($p_1$). The multiple plateaus observed after 72 hours of exposure in the three highest concentrations indicate that the resistant subpopulation ($p_2$) has a tail of more resistant cells with higher threshold for initiation of drug-induced cell death. **E,** EMMA's mathematical representation of the threshold for induction of cell death depicts two distributions: the first, more sensitive, is almost uniform, whereas the second, more resistant, is represented by a wider distribution. **F,** EMMA's quantification of rate of drug-induced cell death for both subpopulations.
For more details on model implementation, please refer to the Mathematical Model Description section.

Published OnlineFirst April 11, 2017; DOI: 10.1158/0008-5472.CAN-17-0502



**Table 1.** Patient demographics, correlation between model predictions and clinical outcome according to IMWG, and theoretical best outcome based on model predictions of best therapy

| Patient ID | Age | Gender | Status at Bmbx | Actual treatment | Actual response/no response | Model's prediction response/no response | Actual outcome (last M-Spike available) | Model's outcome (last M-Spike available) |
|---|---|---|---|---|---|---|---|---|
| 6 | 68 | M | PD | PI+IMID | NR | NR | PD/SD | PD/SD |
| 7 | 76 | M | PD | PI+ALK+IMID | NR | NR | PD/SD | PD/SD |
| 9 | 51 | F | PD | PI+IMID | NR | NR | PD/SD | PD/SD |
| 10 | 56 | F | PD | PI+IMID | R | R | MR/PR | MR/PR |
| 11 | 45 | M | ND | PI+IMID | R | R | VGPR/CR | VGPR/CR |
| 12 | 65 | F | ND | PI+IMID | R | R | VGPR/CR | VGPR/CR |
| 14 | 68 | M | ND | PI+IMID | R | R | VGPR/CR | VGPR/CR |
| 15 | 76 | M | ND | PI+IMID | R | R | VGPR/CR | VGPR/CR |
| 18 | 77 | F | PD | PI+IMID | R | R | MR/PR | VGPR/CR |
| 21 | 63 | M | PD | PI+IMID | NR | NR | PD/SD | PD/SD |
| 24 | 66 | M | ND | PI+IMID | R | R | VGPR/CR | VGPR/CR |
| 27 | 49 | F | PD | PI+IMID | NR | NR | PD/SD | PD/SD |
| 34 | 66 | M | RD | PI+IMID | NR | NR | PD/SD | PD/SD |
| 36* | 51 | F | PD | CRM1i+DOX+DEX | R | R | MR/PR | MR/PR |
| 37 | 69 | M | PD | PI+ALK+IMID | NR | NR | PD/SD | PD/SD |
| 39* | 51 | F | PD | CRM1i+DOX+DEX | R | R | MR/PR | VGPR/CR |
| 47 | 62 | F | PD | PI+IMID | R | R | MR/PR | MR/PR |
| 51** | 49 | F | PD | CRM1i+DOX+DEX | R | R | MR/PR | MR/PR |
| 53 | 53 | M | PD | CRM1i+DOX+DEX | R | R | MR/PR | MR/PR |
| 54 | 62 | M | PD | PI | NR | NR | PD/SD | PD/SD |
| 55 | 71 | M | PD | PI+ALK+IMID | NR | NR | PD/SD | PD/SD |
| 56 | 64 | M | PD | PI+IMID | R | R | MR/PR | MR/PR |
| 57** | 66 | M | PD | CRM1i+DOX+DEX | R | R | MR/PR | VGPR/CR |
| 58 | 68 | F | RFD | PI+IMID | NR | NR | PD/SD | PD/SD |
| 59 | 74 | M | RD | CRM1i+DOX+DEX | R | R | MR/PR | VGPR/CR |
| 64 | 75 | M | PD | PI | NR | NR | PD/SD | PD/SD |
| 68 | 53 | M | PD | CRM1i+DOX+DEX | R | R | MR/PR | MR/PR |
| 69 | 65 | F | PR | PI+ALK+IMID | NR | NR | PD/SD | PD/SD |
| 71 | 74 | M | RD | CRM1i+DOX+DEX | R | R | MR/PR | MR/PR |
| 73 | 64 | F | ND | PI+IMID | R | NR | MR/PR | PD/SD |
| 74 | 63 | M | PD | PI+IMID | R | R | MR/PR | MR/PR |
| 78 | 67 | F | RFD | PI+ALK+IMID | R | R | MR/PR | MR/PR |
| 84 | 67 | M | RFD | CRM1i+DOX+DEX | NR | NR | PD/SD | PD/SD |
| 87 | 76 | M | PD | PI+IMID | R | R | VGPR/CR | MR/PR |
| 94 | 82 | F | ND | PI+ALK+IMID | R | R | VGPR/CR | MR/PR |
| 95 | 56 | F | PD | CRM1i+DOX+DEX | R | NR | MR/PR | PD/SD |
| 97 | 68 | M | PD | ALK (ASCT) | R | R | VGPR/CR | VGPR/CR |
| 98 | 67 | F | PD | PI+IMID | R | R | VGPR/CR | VGPR/CR |
| 100 | 70 | M | PD | PI+IMID | NR | NR | PD/SD | PD/SD |
| 102 | 67 | F | PD | PI+IMID | R | R | MR/PR | MR/PR |
| 103 | 40 | M | ND | PI+IMID | R | R | VGPR/CR | VGPR/CR |
| 105 | 62 | M | ND | PI+IMID | R | R | VGPR/CR | MR/PR |
| 110 | 70 | M | PD | P+D+ACY241 | R | R | MR/PR | MR/PR |
| 111 | 64 | M | ND | K(70)+R+D | R | R | VGPR/CR | VGPR/CR |
| 114 | 52 | M | ND | V+R+D | R | R | MR/PR | MR/PR |
| 119 | 67 | M | RD | K+CY+D | R | R | MR/PR | MR/PR |
| 120 | 58 | M | SMM=>MM | K+R+D | NR | NR | PD/SD | PD/SD |
| 121 | 60 | F | PD | P+D+DARA | R | R | MR/PR | VGPR/CR |
| 122 | 63 | F | PD | V+R+D | R | R | VGPR/CR | VGPR/CR |
| 126 | 65 | F | PD | K+R+D | R | R | MR/PR | VGPR/CR |
| 127 | 58 | F | ND | V+D | R | R | MR/PR | MR/PR |
| 130 | 76 | M | PD | CRM1i+DX+D | R | R | MR/PR | MR/PR |

NOTE: The age range was 40–81, with a median of 65 years old. Biopsies were obtained between April 2014 and July 2016. * and ** indicate sequential biopsies of the same patient.

Abbreviations for disease status: PD, progressive disease; ND, newly diagnosed; RD, relapsed disease; RFD, refractory disease. For treatment: M, marizomib; CFZ, carfilzomib; CY, cyclophosphamide; D, dexamethasone; VD, bortezomib + dexamethasone; VRD, bortezomib + lenalidomide + dexamethasone; OPR, oprozomib; CRD, carfilzomib + lenalidomide + dexamethasone; VPD, bortezomib + pomalidomide + dexamethasone; CyBorD, cyclophosphamide + bortezomib + dexamethasone; V, bortezomib; CFZ + P + D, carfilzomib + pomalidomide + dexamethasone; DX, liposomal doxorubicin. For clinical response: CR, complete response; VGPR, very good partial response; PR, partial response; MR, minimal response; SD, stable disease; PD, progressive disease.

Fig. S6), but anticipated an early relapse, thus classifying this patient at 90 days as nonresponder. Of note, this patient relapsed after 4 months.

***Predictions according to International Myeloma Working Group stratification.*** A more strict level of prediction is used to assess clinical response according to a stratification system aligned with

Published OnlineFirst April 11, 2017; DOI: 10.1158/0008-5472.CAN-17-0502



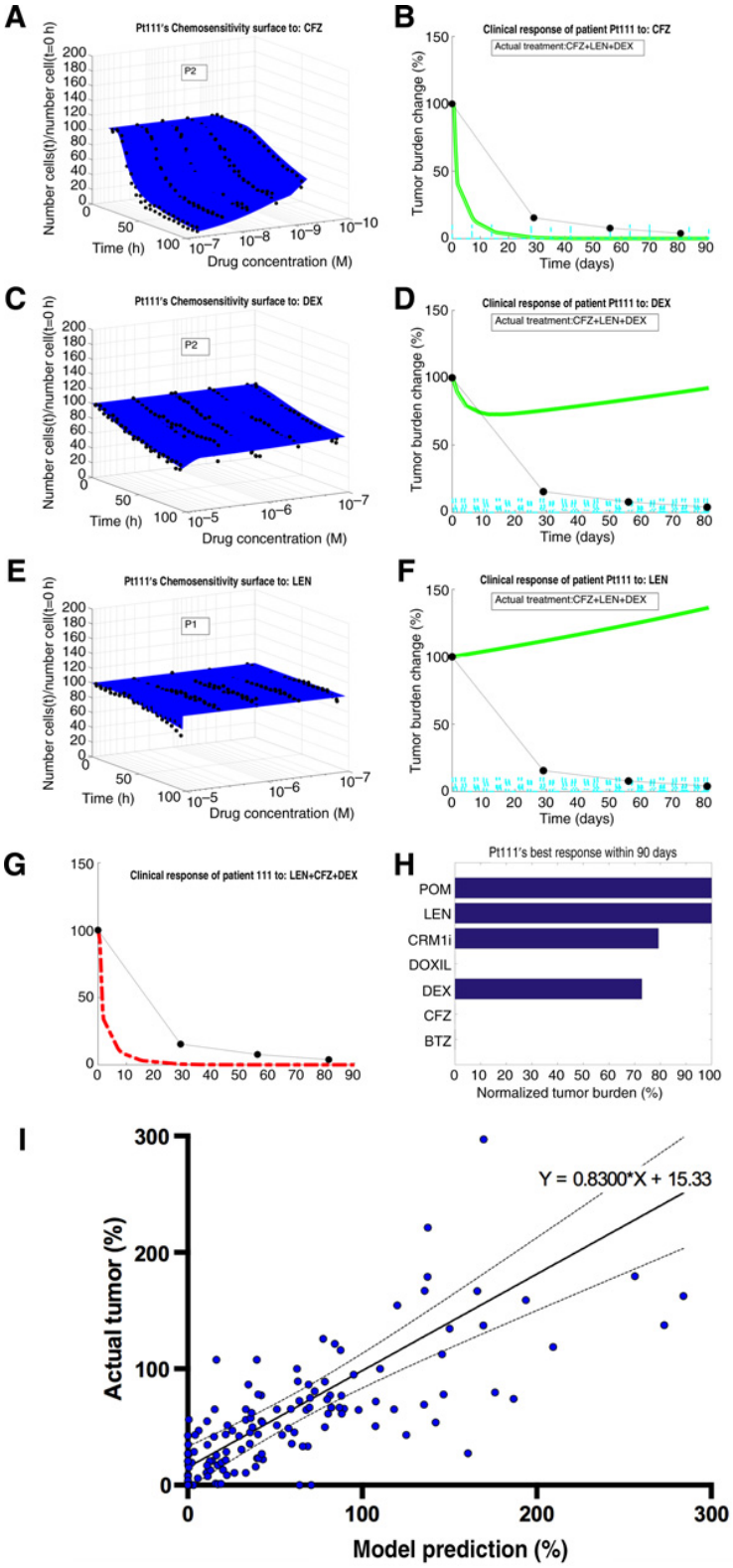


**Figure 3.**

From mathematical model to clinical predictions. **A,** EMMA's mathematical model fitting of patient Pt111's multiple myeloma cells' *ex vivo* response to carfilzomib (CFZ) indicates the presence of two "clonal" (no distribution) subpopulations. **B,** The simulation of the patient-specific mathematical model using published phase I trial pharmacokinetic data generates a prediction curve of clinical response. The actual response of the patient, as measured by serum paraprotein, is overlaid as black dots linked by dashed lines. The same process was followed for the two other drugs in the regimen, dexamethasone (DEX; **C** and **D**) and lenalidomide (LEN; **E** and **F**). By combining the effect of the three drugs assuming additivity, EMMA creates the actual clinical prediction of the patient's estimated response to the therapeutic regimen (**G**). **H,** An analysis of the clinical efficacy (lowest achievable tumor burden, normalized by treatment initiation) shows that carfilzomib, bortezomib, and liposomal doxorubicin are the most active agents, with a prediction of 100% tumor reduction, followed by dexamethasone (27% tumor reduction) and CRM1i (21% reduction). Lenalidomide and pomalidomide had no predicted effect. **I,** Tumor burden measures from each of the patients in this study (133 in total, detailed in Supplementary Fig. S6) were correlated with the corresponding model prediction. The linear regression indicates high correlation between model predictions and actual outcome (equation of regression line Actual = 0.8300*Model+15.33, Pearson $r = 0.5658$, $P < 0.0001$).

Published OnlineFirst April 11, 2017; DOI: 10.1158/0008-5472.CAN-17-0502



the International Myeloma Working Group (IMWG) multiple myeloma response criteria (27), which clusters patient responses in three categories: VGPR/CR includes complete response (>99% tumor reduction) or very good partial response (90%–99% reduction), MR/PR includes partial response (50%–90% reduction) or minimal response (25%–50% reduction), and PD/SD, which includes stable disease (<25% reduction) or progressive disease (>25% increase). Table 1 outlines the postbiopsy therapy received by each patient in this study, corresponding clinical outcome according to the IMWG response criteria (28), and EMMA's predictions. Model predictions and clinical outcome agreed in 41 of 52 patients (79%). The highest accuracy occurred when the model predictions were PD/SD (15/17, or 88% accuracy), followed by MR/PR (16/19, or 84% accuracy) and VGPR/CR (10/16, or 63% accuracy). The narrower the range of response in each category, the greater the chance of disagreement between model predictions and actual outcome. Therefore, a more natural validation of EMMA would be a direct correlation between the actual tumor burden measures and model predictions as continuous variables.

***Linear correlation between predicted and actual tumor burden.*** The strictest validation of this model is the direct correlation of the tumor burden predictions with all available tumor burden measurements. Supplementary Fig. S6 highlights the model predictions and actual tumor burden measurements from 52 patients. Each graph shows tumor burdens normalized by the date of beginning of treatment post-biopsy (i.e., tumor burden = 100% at time = 0 days). Thick-colored lines represent model predictions of clinical response generated 5 days after biopsy. Each prediction curve is flanked by thinner lines, representing the upper and lower boundaries of the prediction. These boundaries are a function of low and high estimates of tumor growth rate, computed from prebiopsy measures of tumor burden. Black dots linked by dashed lines represent the patient's clinical after biopsy tumor burden measurements. Figure 3I shows the aggregated correlation between mathematical model predictions and actual clinical response for all available tumor burden measurements from the 52 patients within 90 days after biopsy (133 data points). The regression line between *in silico* model predictions and clinical response, shown flanked by the 95% confidence interval, had a slope of 0.83 and Pearson correlation coefficient $r = 0.5658$ ($P < 0.0001$).

**Estimated clinical benefit of EMMA as a decision-support system for choice of therapy**

As a multi-drug predictive biomarker, EMMA has two main goals: (i) to ensure that each patient receives the most effective therapy and (ii) to remove ineffective drugs from therapy. According to the model predictions, if EMMA's choice of drugs was used, the number of patients in this study who achieved VGPR or CR would have increased from 13 to 22, the number of patients presenting MR or PR would have decreased from 24 to 23, and the number of patients with no clinical benefit (PD or SD) would have decreased from 15 to 7. Also, according to EMMA, 60% of patients in this study received at least one agent with no predicted clinical efficacy (Supplementary Table S2). As an estimate of the single-agent efficacy of the drugs administered to these 52 patients, EMMA predicted that 34% of the agents had no predicted clinical efficacy, 24% were predicted to produce stable disease, 27% a minimum or partial response, and 15% a very good or complete response. These data suggest the potential clinical benefit of identifying the right drug for the right patient at the right time.

**A high-throughput tool for personalized drug screening**

We have tested the sensitivity of primary multiple myeloma cells from 13 patient samples to a panel of 5 anti–multiple myeloma agents and 25 PKIs. In Fig. 4A, each cell of the heatmap represents the average 96-hour AUC of the five concentrations (1:3 serial dilution, two replicates each) for each drug in individual patients. The drugs were ordered from lowest to highest AUC averaged across all patients, green being the most effective and red the least effective. Figure 4B lists the previous lines of therapy. Despite interpatient variation, it is possible to identify PKIs with consistently higher activity (e.g., BI2536, INK128, ponatinib, MK2206, and crizotinib), whereas others are consistently ineffective (e.g., ralimetinib, vemurafenib, VX745, and BMS777607). Further, PKIs that demonstrated patient-specific activity (*e.g.*, ibrutinib, momelotinib, AZD1480, and palbociclib) highlight the potential for personalized management strategies. For example, the multidrug refractory patients 79 and 83 demonstrated sensitivity to the FDA-approved BTK inhibitor ibrutinib, suggesting that these two patients may derive clinical benefit from treatment with this PKI. The remaining patients were resistant to ibrutinib, further illustrating the need for personalized strategies for treatment allocation. These data indicate that this approach may be used to assess patient sensitivity to targeted therapeutics facilitating patient sample–derived drug screening or *in silico* clinical trials of experimental agents.

In addition, by grouping the 30 agents in pairs and performing a linear regression in each of the possible 435 combinations, it was possible to investigate agents with putative *ex vivo* activity correlation (Supplementary Fig. S7). Fifteen pairs of drugs showed Pearson correlation coefficient $r > 0.75$, suggesting that their anti–multiple myeloma activities involved similar biological processes in these patient specimens. Certain pairs were consistent with known activities such as carfilzomib/bortezomib and bortezomib/panobinostat, which have established links in anti–multiple myeloma activities (29). Other pairs, including panobinostat (HDACi)/ponatinib (Abli), with a positive slope of 0.8755 and $r = 0.7695$, suggest previously undefined shared biological pathways contributing to multiple myeloma survival. Interestingly, there were no instances of drugs with significant interpatient inverse correlation. This suggests that, across a group of patients, increased resistance to one drug during treatment correlates with increase, or has no effect at all, on resistance to a second drug, while cross-sensitization between drugs is unlikely (Supplementary Fig. S8). This has been observed in multiple clinical trials of alternating therapies seeking to exploit a cost of adaptation to two different regimens (30). Ultimately, those studies failed to demonstrate a significant improvement in survival between sequential and alternating groups (31, 32). However, our data suggest that there are patient-specific exceptions to this rule. For instance, Supplementary Fig. S9 depicts changes in 96-hour LD50 values for 2 patients between two sequential biopsies for 20 PKIs, with the posttreatment tumors becoming more resistant to some PKIs and, importantly, more sensitive to others, including the clinically relevant crizotinib and ponatinib, as well as the PLK inhibitor BI2536 (33), once again, highlighting the potential for phenotypically derived biomarker tools for truly personalized management.

Published OnlineFirst April 11, 2017; DOI: 10.1158/0008-5472.CAN-17-0502



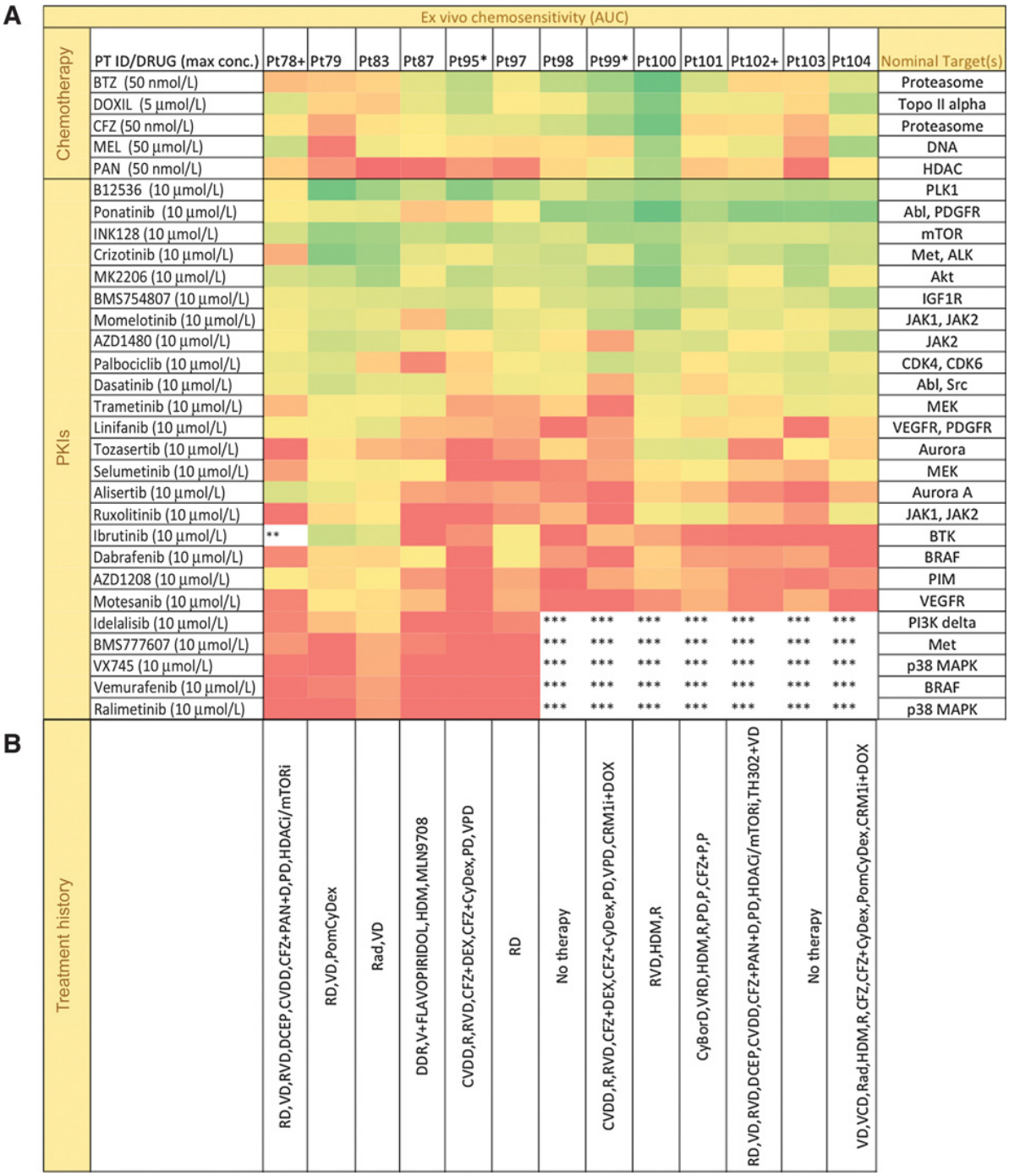


**Figure 4.**

*Ex vivo* chemosensitivity of 13 patient samples to a panel of 25 PKIs and chemotherapeutic agents. **A,** Each sample was tested *ex vivo* in coculture with stroma for 96 hours against 6 chemotherapeutic agents and 25 PKIs at five concentrations. Chemosensitivity was quantified as the normalized AUC for all five concentrations. Drugs were sorted descending order by decreasing activity, with most active drugs represented as green and least active as red. * or + represent patients with sequential biopsies. **, Maximum concentration of drug was 6 µmol/L. ***, Drug not tested. **B,** The list of previous treatments: lenalidomide (R), dexamethasone (D or Dex), bortezomib (V), dexamethasone + cyclophosphamide + etoposide + cisplatin (DCEP), cyclophosphamide + bortezomib + liposomal doxorubicin + dexamethasone (CVDD), carfilzomib (CFZ), panobinostat (PAN), pomalidomide (POM or P), liposomal doxorubicin + dexamethasone + lenalidomide (DDR), high-dose melphalan followed by bone marrow transplant (HDM), cyclophosphamide (Cy), radiation (Rad), cyclophosphamide + bortezomib + dexamethasone (CyBorD), and pomalidomide + dexamethasone (PD).

Published OnlineFirst April 11, 2017; DOI: 10.1158/0008-5472.CAN-17-0502



Critically, even drugs within a same class, such as bortezomib and carfilzomib, can have significantly different clinical efficacy. Carfilzomib has been shown to be the more effective PI in early relapsed multiple myeloma (34); however, from Supplementary Table S2, Fig. 5, and Supplementary Fig. S10, it is clear that individual patients have differential predicted sensitivities to one PI versus the other. For instance, 7 of the 21 patients predicted as resistant to bortezomib were predicted to respond to carfilzomib. In contrast, 10 of the 24 patients predicted as resistant to carfilzomib were predicted to respond to bortezomib. Despite correlated *ex vivo* activity (Supplementary Fig. S7), the two drugs have different PK, leading to different predicted clinical responses. Collectively, these data again illustrate the potential clinical importance of allocating the right drug to the right patient at the right time even within a class of agents.

**A platform for *in silico* clinical trials**

We have tested 19 patient samples (Supplementary Table S3) with the HDAC6 inhibitor ricolinostat (Ri) and the Bcl-2 inhibitor venetoclax (Ve), created patient-specific models of chemosensitivity and simulated how these patients would have responded in a clinical trial. We have compared our results with actual phase I/II studies with single agents and combination with bortezomib (V) and dexamethasone (D; refs. 35, 36). The only data used for the simulations were the *ex vivo* results and drug-specific PK. The results are depicted in Fig. 6: in the single agent ricolinostat arm of the *in silico* trial (Fig. 6A), 1 patient (5%) was predicted to achieve VGPR/CR, 1 patient (5%) would achieve MR, whereas the remaining 17 (90%) would present PD/SD, in agreement with the low single-agent efficacy observed in the actual trial (60% PD and 40% SD). The simulation of single-agent venetoclax (Fig. 6B) predicted 3 patients reaching VGPR/CR (17%), 3 reaching PR (17%), 3 reaching MR (17%), and 9 presenting PD/SD (50%). Consistent with the clinical activity of venetoclax in phase I trials (36), t(11,14) status correlated with EMMA-predicted drug sensitivity with a mean depth of response 60% versus 31% of t(11,14) positive versus negative multiple myeloma, respectively ($P = 0.0275$). Note that newly diagnosed status (NDMM) was also a predictor of response (Fig. 6B, inset). It is also important to note that responses and failures were noted in both groups as well, demonstrating that molecular screening alone would not adequately predict clinical outcome. The virtual trial also projected clinical benefit for adding either drug to bortezomib and dexamethasone (V+D, $P = 0.0181$ and $P = 0.0175$ for Ri for Ve, Fig. 6C and D, respectively). Again, the actual benefit is observed in only a percentage of patients, highlighting the potential for the utilization of a phenotypic biomarker screening prior to treatment.

## Discussion

Multiple myeloma is an example of a cancer in which the efforts of basic, translational, and clinical research have provided a growing number of therapeutics with significant improvements in survival. Yet, curative intent therapy remains elusive. To this end, it is critical that we best allocate these therapies to maximize outcomes (and ideally minimize toxicities). Here, we have demonstrated a novel approach to predict clinical response of multiple myeloma patients to a wide range of therapeutics using an *ex vivo* chemosensitivity assay and computational models. This assay is scalable, reproducible and allows analysis of drug efficacy in primary multiple myeloma cells in the presence of elements of the tumor microenvironment (matrix, patient-derived serum, and human bone marrow–derived stroma). The major contribution of this approach, compared with existing techniques, is the detailed *ex vivo* characterization of the heterogeneity of tumor chemosensitivity, and its integration with mathematical models to accurately and reproducibly predict clinical response, with the potential to improve patient clinical outcomes through model-informed personalized management decisions.

EMMA has a number of advantages compared with past and current preclinical chemosensitivity assays. First, similar experiments would have cost and time-prohibitive hurdles in PDX models and may not be concluded in clinically actionable time frame (14). Second, EMMA not only mimics the real-time action of the drug on cancer cells, but mathematical models are used to extrapolate this short-term response into a longer clinical time frame, based on PK data. This trait makes EMMA an attractive system for multiple myeloma patients, including multi-drug refractory patients requiring salvage therapy. Third, patient-specific EMMA mathematical models can be used to test the effect of multiple classes of drugs in different regimens, leading to the assignment of the most efficacious regimen or drug to individual patients (21). Finally, EMMA's output is not limited to a dichotomized response/no-response or depth of response, but trajectories of actual clinical response at any moment during the first 3 months of treatment. Thus, its predictions can be followed in real-time during treatment, giving both physician and patient the opportunity to make informed, pretreatment decisions, and proactively act during therapy.

Recent works in the field have suggested different approaches to identify agents with clinical efficacy in liquid and solid cancers. Pemvoska and colleagues (4) have described a combination of *ex vivo* chemosensitivity and molecular profiling to determine therapeutic windows for drugs in acute myeloid leukemia. Majumder and colleagues have combined *ex vivo* chemosensitivity assays of slices of tumor explants (37), immunohistochemistry, and clinical data to create a signature to classify clinical response of patients with solid tumors. Both methods assess chemosensitivity at one fixed time point and do not account for the temporal dynamics of cell death, essential for the extrapolation of the effect of short periods of drug exposure (*in vitro*) to actual clinical response. In an analogy to physical sciences, these assays are capable of determining the initial speed of the clinical response but not "acceleration" and thus cannot predict the clinical trajectory. The concept of "acceleration" implies that the response of cancer cells to therapy cannot be described as a first-order differential equation, where rate of cell death is proportional to drug concentration, but instead requires a second-order model, which incorporates the notion of "damage," and a threshold beyond which cell death starts. To this end, other assays can predict the initial effect of therapy on tumor burden, but cannot predict the actual depth, duration, or time to relapse. In cancers such as multiple myeloma, depth of response is commonly utilized as surrogates of clinical benefit (38). As such, a system capable of creating actual clinical trajectories (response) will be central to successfully translating *in silico* predictions to true clinical outcomes. In addition, although the agnostic pattern recognition techniques used in these published works (37) are adequate to

Published OnlineFirst April 11, 2017; DOI: 10.1158/0008-5472.CAN-17-0502



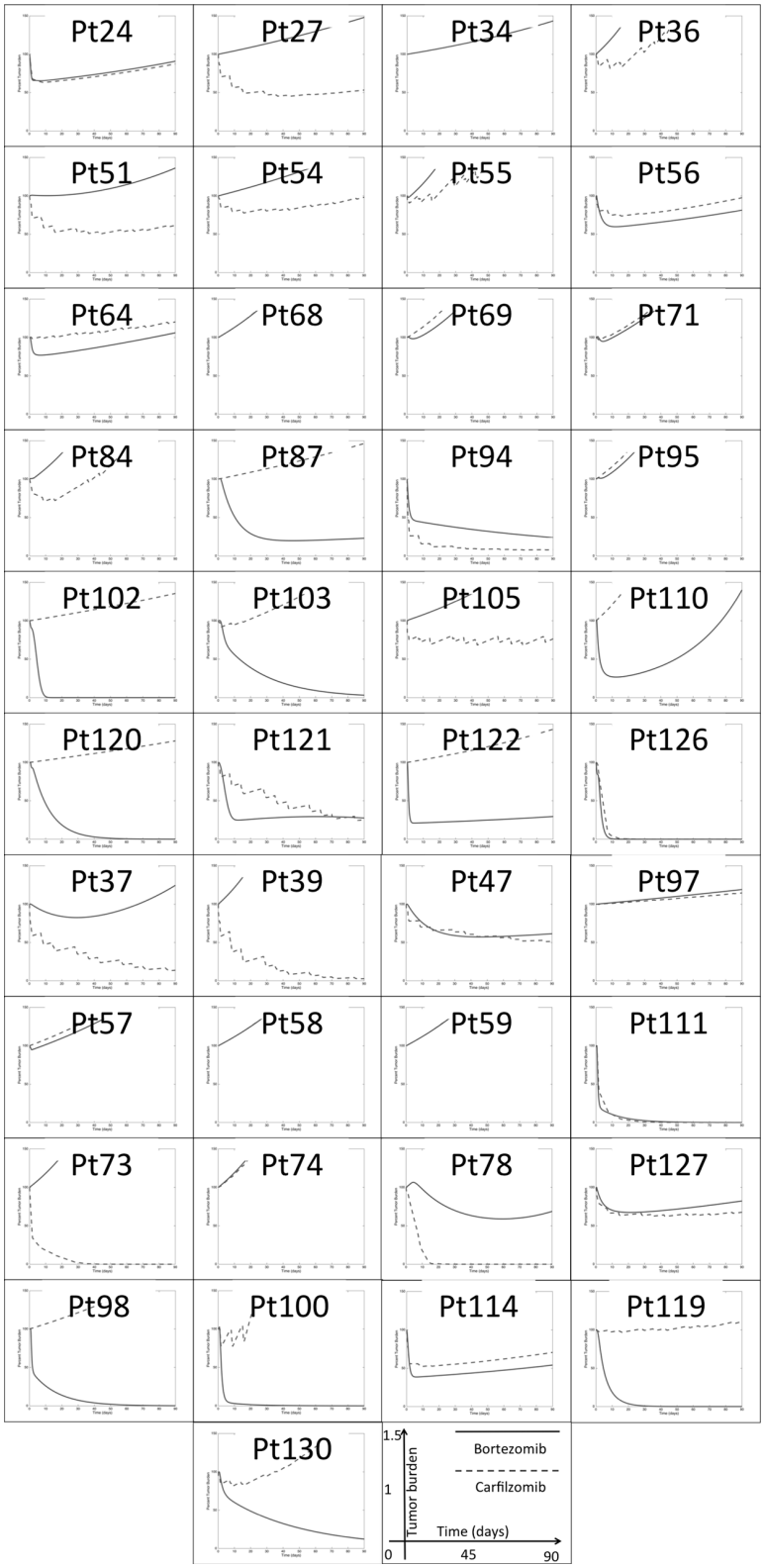


**Figure 5.**
Model predictions of clinical response of 41 multiple myeloma patients indicate no correlation between bortezomib and carfilzomib 90-day depth of response. Each graph represents the model-predicted clinical response to bortezomib (blue solid line) and carfilzomib (red dashed line) as single agents during an interval of 90 days. The vertical axis, ranging from 0% to 150%, represents the tumor burden values as a percentage of the pretreatment tumor (day 0).

Published OnlineFirst April 11, 2017; DOI: 10.1158/0008-5472.CAN-17-0502



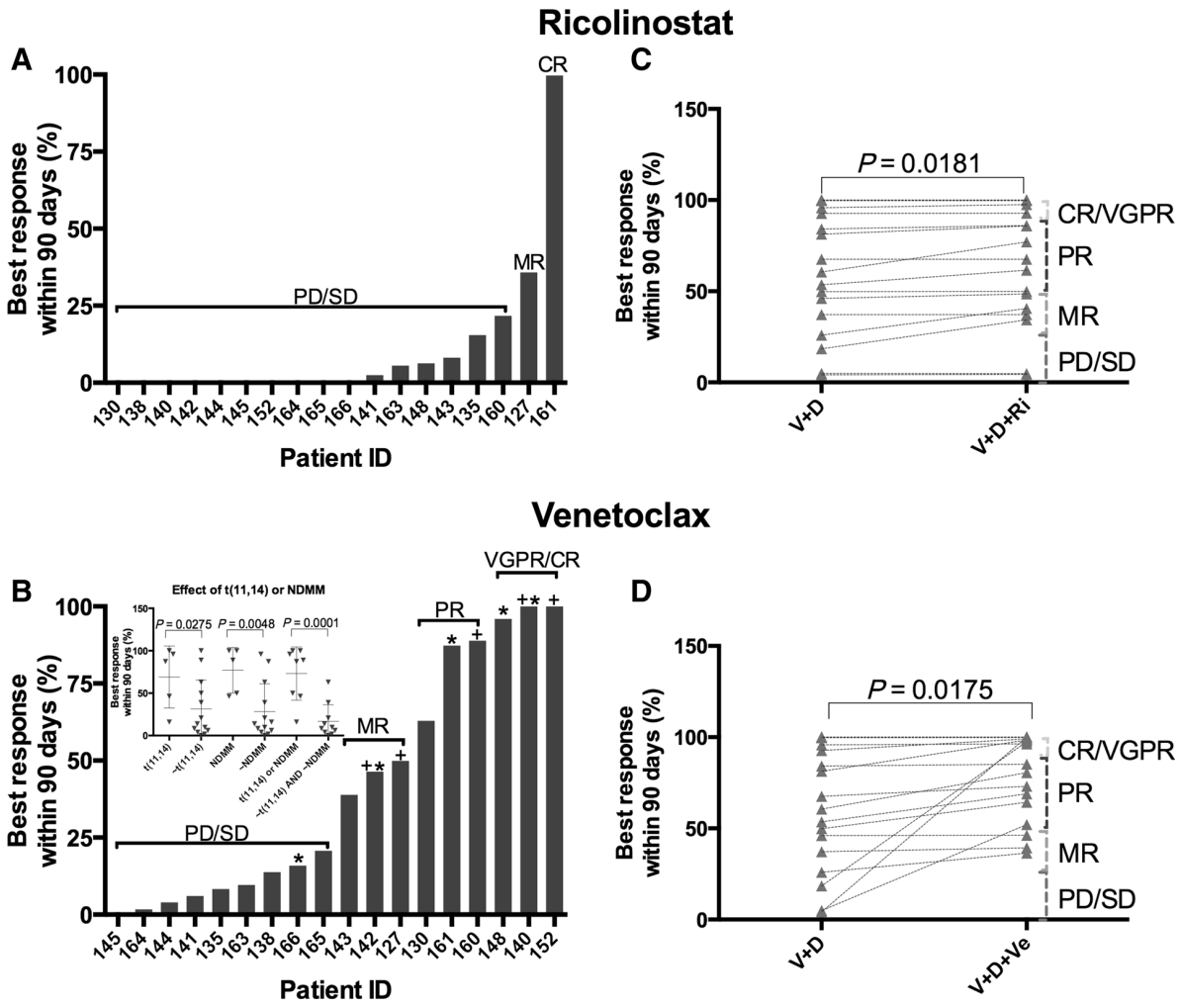


**Figure 6.**

Virtual clinical trial of ricolinostat and venetoclax as single agents and combination with bortezomib and dexamethasone. We have used EMMA to simulate the clinical response of 19 multiple myeloma patients to the HDAC6 inhibitor ricolinostat (160 mg days 1–5 and 8–12 on a 21-day cycle) and the BCL-2 inhibitor venetoclax (1,200 mg daily) as single agents and in combination with bortezomib and dexamethasone. **A** and **B** represent each of the patients' maximum response to either drug as single agents during 90 days, 100% indicating complete tumor regression and 0% indicating no tumor reduction. **C** and **D** indicate each patient's expected response to either drug's combinations with bortezomib and dexamethasone (V+D, V+D+Ri, and V+D+Ve). Statistical differences were observed as a consequence of the inclusion of ricolinostat (two-tailed paired *t* test, $P = 0.0181$) and venetoclax (two-tailed paired *t* test, $P = 0.0175$), despite limited single-agent activities in most patients. Presence of translocation 11,14 or newly diagnosed status correlated with sensitivity to single-agent venetoclax (inset B). t(11,14) stands for positive for translocation between chromosomes 11 and 14, NDMM stands for newly diagnosed, ~ stands for "not," thus "~NDMM" stands for not newly diagnosed. *t(11,14) positive, +newly diagnosed.

create signatures capable of classifying patients into categories such as responders or nonresponders, they lack the ability to extrapolate conditions for which the signature was not trained. For instance, how would a patient respond to a combination of two drugs for which signatures were predetermined, or a different therapeutic regimen (dosing and schedule) for a known drug? The novel approach developed in this work provides an instrumental platform to address these issues. So far, EMMA-generated clinical predictions for regimens of two or more drugs assume additivity, which is the simplest possible implementation. However, our preliminary data indicate regions in the time–concentration space where there is synergy in primary multiple myeloma cells treated *ex vivo* (Supplementary Materials and Methods and Supplementary Fig. S11). Given drug-specific PK, staggered drug administration schedules, and the inherent heterogeneity of tumor populations, further work is required to adequately incorporate this information in EMMA models.

Predicting clinical response of patients based on *ex vivo* assays is a major challenge irrespective of how close the assay is to *in vivo* conditions. The most obvious difficulty is the translation of results from an assay that lasts for days into estimates of clinical response across months or even years (1, 38). We have begun to bridge this timescale gap through the use of mathematical models

Published OnlineFirst April 11, 2017; DOI: 10.1158/0008-5472.CAN-17-0502



accounting for tumor heterogeneity, pharmacodynamics, and PK imputed with a tested phenotype (drug sensitivity). It has been long known that nature selects for phenotype, not genotype, and that multiple genotypes can produce the same phenotype (39). This nonexclusive relationship makes it challenging to predict clinical outcome from genotype alone or even gene expression profiles (40). EMMA directly identifies the phenotypic (or functional) representation of subpopulations regardless of genotypic background, thus removing the "middle man" and producing *in silico* clinical response outputs. Through nonlinear regression of the *ex vivo* chemosensitivity results, the model identifies subpopulations within the tumor burden based on chemosensitivity. In turn, the platform combines these data with drug- and regimen-specific PK, generating trajectories of clinical response demonstrating a high degree of accuracy in predicting outcomes.

We anticipate that this approach can provide precise clinical insight about treatment efficacy in a timely manner and assist oncologists in practicing truly personalized management, by proposing the best choice of therapy for each patient and identifying those with risk of early relapse due to the presence of therapy-resistant cells. In addition to clinical predictions of standard-of-care regimens, this approach can also serve as a means to perform *in silico* clinical trials (Fig. 6; refs. 5, 41, 42), where several experimental agents are tested in primary multiple myeloma cells from a cohort of patients mimicking the actual clinical setting without the potential cost or toxicity to patients. Additional uses of these mathematical models include the simulation of alternative regimens, such as metronomic therapy (43), adaptive therapy (44), or the introduction of treatment "holidays" (45), depending on the nature of the mechanism of resistance. Once the subpopulations have been identified and characterized by this method, computer simulations can be used to determine which alternative regimens may lead to best clinical outcome (45, 46).

Importantly, the mechanistic nature of these computational models allows the incorporation of additional influences on clonal evolution, including genotypic, epigenetic, microenvironmental, and clinical data, to continually upgrade this system. To this end, we expect to continue to build additional parameters into this computational model to improve the predictive capacity and to account for new classes of therapeutics. Studies are underway to integrate our prior models of response trajectories (47, 48) with EMMA to move from predications of depth of response to PFS. Further, we recognize the increasing importance of immune-mediated therapies in multiple myeloma (49, 50). Our preliminary studies with the CD38 antibody daratumumab (50), using EMMA's current protocol, have shown activity in primary multiple myeloma cells in concentrations as low as 86 nmol/L, with cell death initiated after 4 days, and reaching 25% viability reduction 1 day later. As depicted in Supplementary Fig. S12, the mechanism of cell death is phagocytosis by a yet-to-be-determined adherent cell present in the coculture, and only occurs in the presence of daratumumab. Research is ongoing to parameterize T-cell, NK-cell, and myeloid-derived stromal cell phenotypes in patient bone marrow samples to direct T-cell cytotoxicity assays in this platform. We anticipate that these data can be incorporated in EMMA to account for sensitivity to specific immune-based therapies. Further, continued validation of inter-day reproducibility (Supplementary Fig. S13), intra-plate variation (Supplementary Fig. S14), and dependence of AIC convergence of solution on *ex vivo* experiment duration and dynamic range of drug concentration (Supplementary Fig. S15, Supplementary Table S4, Supplementary Fig. S16, Supplementary Table S5, and Supplementary Figs. S17 and S18) are ongoing in larger numbers of patients to achieve the goal of a true clinical decision support tool.

To our knowledge, this study provides estimates on the individual efficacy of clinically administered agents in multiple myeloma for the first time: approximately one third of agents administered in this study may have had little to no clinical efficacy, 60% of patients received at least one ineffective agent, and 31% could have been treated with a more effective agent proposed by the mathematical models. Thus, we anticipate that EMMA would provide a critical support to oncologists to customize regimens by avoiding therapeutics that will not benefit the patient, thus reducing the potential toxicity while maximizing the clinical benefit.

## Disclosure of Potential Conflicts of Interest

R. Baz reports receiving commercial research grant from Celgene, Karyopharm, Merck, Millennium, and Millenium/Takeda. K.H. Shain reports receiving commercial research grant from AbbVie and Signal Genetics, received honoraria from the Speakers Bureau of Amgen, Celgene, Janssen, Novartis, and Takeda, and is a consultant/advisory board member for Amgen, Celgene, Janssen, and Takeda. No potential conflicts of interest were disclosed by the other authors.

## Authors' Contributions

**Conception and design:** A. Silva, P. Sudalagunta, T. Jacobson, J. Song, R. Baz, W. Dalton, R. Gatenby, R. Gillies, E. Sontag, K.H. Shain
**Development of methodology:** A. Silva, M.C. Silva, P. Sudalagunta, T. Jacobson, C. Cubitt, W. Dalton, E. Sontag, M.B. Meads, K.H. Shain
**Acquisition of data (provided animals, acquired and managed patients, provided facilities, etc.):** A. Silva, M.C. Silva, A. Distler, T. Nguyen, C. Cubitt, R. Baz, L. Perez, W. Dalton, M.B. Meads, K.H. Shain
**Analysis and interpretation of data (e.g., statistical analysis, biostatistics, computational analysis):** A. Silva, M.C. Silva, P. Sudalagunta, T. Jacobson, D.-T. Chen, L. Chen, R. Baz, J. Greene, R. Gillies, E. Sontag, M.B. Meads, K.H. Shain
**Writing, review, and/or revision of the manuscript:** A. Silva, M.C. Silva, P. Sudalagunta, T. Jacobson, J. Song, C. Cubitt, R. Baz, L. Perez, D. Rebatchouk, W. Dalton, R. Gatenby, R. Gillies, E. Sontag, M.B. Meads, K.H. Shain
**Administrative, technical, or material support (i.e., reporting or organizing data, constructing databases):** A. Collins, C. Cubitt, W. Dalton, K.H. Shain
**Study supervision:** A. Silva, K.H. Shain

## Acknowledgments

The authors thank the patients at H. Lee Moffitt Cancer Center who provided clinical samples for our *ex vivo* assays as well as consented access to the their clinical data through the Total Cancer Care database.

## Grant Support

This research was funded by the H. Lee Moffitt Cancer Center Physical Sciences in Oncology (PSOC) Grant (1U54CA193489-01A1) and by H. Lee Moffitt Cancer Center's Team Science Grant. This work has been supported in part by the Translational Research Core Facility at the H. Lee Moffitt Cancer Center & Research Institute, a NCI-designated Comprehensive Cancer Center (P30-CA076292). Access to primary cells was made possible through the Total Cancer Care Protocol at the Moffitt Cancer Center.

The costs of publication of this article were defrayed in part by the payment of page charges. This article must therefore be hereby marked *advertisement* in accordance with 18 U.S.C. Section 1734 solely to indicate this fact.

Received February 21, 2017; revised April 7, 2017; accepted April 7, 2017; published OnlineFirst April 11, 2017.

Published OnlineFirst April 11, 2017; DOI: 10.1158/0008-5472.CAN-17-0502



## References


1. Suggitt M, Bibby MC. 50 years of preclinical anticancer drug screening: Empirical to target-driven approaches. Clin Cancer Res 2005;11: 971–81.
2. Montero J, Sarosiek KA, DeAngelo JD, Maertens O, Ryan J, Ercan D, et al. Drug-induced death signaling strategy rapidly predicts cancer response to chemotherapy. Cell 2015;160:977–89.
3. Rubio-Perez C, Tamborero D, Schroeder MP, Antolin AA, Deu-Pons J, Perez-Llamas C, et al. In silico prescription of anticancer drugs to cohorts of 28 tumor types reveals targeting opportunities. Cancer Cell 2015;27: 382–96.
4. Pemovska T, Kontro M, Yadav B, Edgren H, Eldfors S, Szwajda A, et al. Individualized systems medicine strategy to tailor treatments for patients with chemorefractory acute myeloid leukemia. Cancer Discov 2013;3: 1416–29.
5. Khin ZP, Ribeiro ML, Jacobson T, Hazlehurst L, Perez L, Baz R, et al. A preclinical assay for chemosensitivity in multiple myeloma. Cancer Res 2014;74:56–67.
6. Meads MB, Gatenby RA, Dalton WS. Environment-mediated drug resistance: A major contributor to minimal residual disease. Nat Rev Cancer 2009;9:665–74.
7. Stewart AK, Rajkumar SV, Dimopoulos MA, Masszi T, Spicka I, Oriol A, et al. Carfilzomib, lenalidomide, and dexamethasone for relapsed multiple myeloma. N Engl J Med 2015;372:142–52.
8. Shargel L, Wu-Pong S, Yu ABC. Applied biopharmaceutics & pharmacokinetics. 5th ed. New York, NY: Appleton & Lange Reviews/McGraw-Hill, Medical Pub. Division; 2005.
9. Clark AJ. The reaction between acetyl choline and muscle cells. Part II. J Physiol 1927;64:123–43.
10. Akaike H. A new look at the statistical model identification. IEEE Trans Automat Contr 1974;19:716–23.
11. Ghobrial IM, Weller E, Vij R, Munshi NC, Banwait R, Bagshaw M, et al. Weekly bortezomib in combination with temsirolimus in relapsed or relapsed and refractory multiple myeloma: A multicentre, phase 1/2, open-label, dose-escalation study. Lancet Oncol 2011; 12:263–72.
12. Andrulis M, Lehners N, Capper D, Penzel R, Heining C, Huellein J, et al. Targeting the BRAF V600E mutation in multiple myeloma. Cancer Discov 2013;3:862–9.
13. Zhao X, Lwin T, Silva A, Shah B, Tao J, Fang B, et al. Unification of tumor microenvironment (TME) mediated and acquired ibrutinib resistance in mantle cell lymphoma. Nat Commun 2017. PMID: 28416797.
14. Yaccoby S, Barlogie B, Epstein J. Primary myeloma cells growing in SCID-hu mice: A model for studying the biology and treatment of myeloma and its manifestations. Blood 1998;92:2908–13.
15. Das R, Strowig T, Verma R, Koduru S, Hafemann A, Hopf S, et al. Microenvironment-dependent growth of preneoplastic and malignant plasma cells in humanized mice. Nat Med 2016;22:1351–7.
16. Silva A, Jacobson T, Meads M, Distler A, Shain K. An organotypic high throughput system for characterization of drug sensitivity of primary multiple myeloma cells. J Vis Exp 2015;e53070.
17. Najar M, Rouas R, Raicevic G, Boufker HI, Lewalle P, Meuleman N, et al. Mesenchymal stromal cells promote or suppress the proliferation of T lymphocytes from cord blood and peripheral blood: The importance of low cell ratio and role of interleukin-6. Cytotherapy 2009;11:570–83.
18. Wang Z, Yang J, Kirk C, Fang Y, Alsina M, Badros A, et al. Clinical pharmacokinetics, metabolism, and drug-drug interaction of carfilzomib. Drug Metab Dispos 2013;41:230–7.
19. Collins GS, Reitsma JB, Altman DG, Moons KG. Transparent reporting of a multivariable prediction model for individual prognosis or diagnosis (TRIPOD): The TRIPOD statement. Ann Intern Med 2015; 162:55–63.
20. Reece DE, Sullivan D, Lonial S, Mohrbacher AF, Chatta G, Shustik C, et al. Pharmacokinetic and pharmacodynamic study of two doses of bortezomib in patients with relapsed multiple myeloma. Cancer Chemother Pharmacol 2011;67:57–67.
21. Berenson JR, Cartmell A, Bessudo A, Lyons RM, Harb W, Tzachanis D, et al. CHAMPION-1: A phase 1/2 study of once-weekly carfilzomib and dexamethasone for relapsed or refractory multiple myeloma. Blood 2016;127:3360–8.
22. Aljitawi OS, Ganguly S, Abhyankar SH, Ferree M, Marks R, Pipkin JD, et al. Phase IIa cross-over study of propylene glycol-free melphalan (LGD-353) and alkeran in multiple myeloma autologous transplantation. Bone Marrow Transplant 2014;49:1042–5.
23. Pisano C, Cecere SC, Di Napoli M, Cavaliere C, Tambaro R, Facchini G, et al. Clinical trials with pegylated liposomal Doxorubicin in the treatment of ovarian cancer. J Drug Deliv 2013;2013:898146.
24. Harousseau JL, Avet-Loiseau H, Attal M, Marit G, Caillot D, Hulin C, et al. High complete and very good partial response rates with bortezomib-dexamethasone as induction prior to ASCT in newly diagnosed patients with high-risk myeloma: Results of the IFM2005-01 phase 3 trial. Blood 2009;114:149–50.
25. Richardson PG, Weller E, Lonial S, Jakubowiak AJ, Jagannath S, Raje NS, et al. Lenalidomide, bortezomib, and dexamethasone combination therapy in patients with newly diagnosed multiple myeloma. Blood 2010;116:679–86.
26. Li Y, Xu Y, Liu L, Wang X, Palmisano M, Zhou S. Population pharmacokinetics of pomalidomide. J Clin Pharmacol 2015;55:563–72.
27. Kumar S, Paiva B, Anderson KC, Durie B, Landgren O, Moreau P, et al. International Myeloma Working Group consensus criteria for response and minimal residual disease assessment in multiple myeloma. Lancet Oncol 2016;17:e328–46.
28. Chng WJ, Dispenzieri A, Chim CS, Fonseca R, Goldschmidt H, Lentzsch S, et al. IMWG consensus on risk stratification in multiple myeloma. Leukemia 2014;28:269–77.
29. Richardson PG, Schlossman RL, Alsina M, Weber DM, Coutre SE, Gasparetto C, et al. PANORAMA 2: Panobinostat in combination with bortezomib and dexamethasone in patients with relapsed and bortezomib-refractory myeloma. Blood 2013;122:2331–7.
30. Gatenby RA, Brown J, Vincent T. Lessons from applied ecology: Cancer control using an evolutionary double bind. Cancer Res 2009;69:7499–502.
31. Morstyn G, Schechter GP, Ihde DC, Carney DN, Eddy JL, Cohen MH, et al. Therapy for multiple myeloma with alternating non-cross-resistant chemotherapy combinations: Heterogeneity of tumor responsiveness. Cancer Treat Rep 1984;68:1439–46.
32. Mateos MV, Martinez-Lopez J, Hernandez MT, Ocio EM, Rosinol L, Martinez R, et al. Sequential vs. alternating administration of VMP and Rd in elderly patients with newly diagnosed MM. Blood 2016;127:420–5.
33. McMillin DW, Delmore J, Negri J, Ooi M, Klippel S, Miduturu CV, et al. Microenvironmental influence on pre-clinical activity of polo-like kinase inhibition in multiple myeloma: Implications for clinical translation. PLoS One 2011;6:e20226.
34. Dimopoulos MA, Moreau P, Palumbo A, Joshua D, Pour L, Hajek R, et al. Carfilzomib and dexamethasone versus bortezomib and dexamethasone for patients with relapsed or refractory multiple myeloma (ENDEAVOR): A randomised, phase 3, open-label, multicentre study. Lancet Oncol 2016; 17:27–38.
35. Vogl DT, Raje NS, Jagannath S, Richardson PG, Hari P, Orlowski RZ, et al. Ricolinostat, the first selective histone deacetylase 6 inhibitor, in combination with bortezomib and dexamethasone for relapsed or refractory multiple myeloma. Clin Cancer Res 2017 Jan 4. [Epub ahead of print].
36. Rajan AM, Kumar S. New investigational drugs with single-agent activity in multiple myeloma. Blood Cancer J 2016;6:e451.
37. Majumder B, Baraneedharan U, Thiyagarajan S, Radhakrishnan P, Narasimhan H, Dhandapani M, et al. Predicting clinical response to anticancer drugs using an ex vivo platform that captures tumour heterogeneity. Nat Commun 2015;6:6169.
38. Durie BG, Jacobson J, Barlogie B, Crowley J. Magnitude of response with myeloma frontline therapy does not predict outcome: Importance of time to progression in southwest oncology group chemotherapy trials. J Clin Oncol 2004;22:1857–63.
39. Puga A, Wallace KB. Molecular biology of the toxic response. Philadelphia, PA: Taylor & Francis; 1999.
40. Amin SB, Yip WK, Minvielle S, Broyl A, Li Y, Hanlon B, et al. Gene expression profile alone is inadequate in predicting complete response in multiple myeloma. Leukemia 2014;28:2229–34.
41. Scott J. Phase i trialist. Lancet Oncol 2012;13:236.
42. Catenacci DV. Next-generation clinical trials: Novel strategies to address the challenge of tumor molecular heterogeneity. Mol Oncol 2015;9: 967–96.

Published OnlineFirst April 11, 2017; DOI: 10.1158/0008-5472.CAN-17-0502




43. Greaves M. Evolutionary determinants of cancer. Cancer Discov 2015; 5:806–20.
44. Gatenby RA, Silva AS, Gillies RJ, Frieden BR. Adaptive therapy. Cancer Res 2009;69:4894–903.
45. Das Thakur M, Salangsang F, Landman AS, Sellers WR, Pryer NK, Levesque MP, et al. Modelling vemurafenib resistance in melanoma reveals a strategy to forestall drug resistance. Nature 2013;494:251–5.
46. Silva AS, Kam Y, Khin ZP, Minton SE, Gillies RJ, Gatenby RA. Evolutionary approaches to prolong progression-free survival in breast cancer. Cancer Res 2012;72:6362–70.
47. Yankeelov TE, Quaranta V, Evans KJ, Rericha EC. Toward a science of tumor forecasting for clinical oncology. Cancer Res 2015;75:918–23.
48. Silva A, Durand S, Ribeiro M, Alsina M, Shain K, Baz R. An evolutionary approach for personalized therapy in multiple myeloma. Appl Math (Irvine) 2016;7.
49. Kronke J, Udeshi ND, Narla A, Grauman P, Hurst SN, McConkey M, et al. Lenalidomide causes selective degradation of IKZF1 and IKZF3 in multiple myeloma cells. Science 2014;343:301–5.
50. Jelinek T, Hajek R. Monoclonal antibodies - A new era in the treatment of multiple myeloma. Blood Rev 2016;30:101–10.

Published OnlineFirst April 11, 2017; DOI: 10.1158/0008-5472.CAN-17-0502

Cancer Research
The Journal of Cancer Research (1916–1930) | The American Journal of Cancer (1931–1940)

AACR American Association for Cancer Research

# An *Ex Vivo* Platform for the Prediction of Clinical Response in Multiple Myeloma

Ariosto Silva, Maria C. Silva, Praneeth Sudalagunta, et al.

*Cancer Res* Published OnlineFirst April 11, 2017.

**Supplementary Material Index:**

## Supplemental Materials and Methods:

***A novel platform for analysis of drug combinations.*** One of the goals of this study was to develop a platform capable of testing a large number of potential therapeutic agents and combinations (clinical utility and drug development), while maintaining the level of detail required by the mathematical model to simulate the clinical efficacy of each agent or combination. For this purpose, regular drug interaction analysis at a fixed time point is not sufficient, as the temporal effect must be captured into the mathematical model. **Supplemental Figures 11a** and **11b** depict the LD50s (concentration required to kill 50% of MM cells) for primary MM cells from two patients to a panel of drugs and combinations. Despite being a useful representation of patient-specific drug efficacy as single agents, these classic bar plots provide only limited interpretation of the dynamics of drug interaction, and they do not incorporate critical time-dependent information. **Supplemental Figures 11c** and **11d** exemplify how this assay can be used to determine the cell-kill benefit of combining two agents. Each image represents normalized drug concentration on the horizontal axis and exposure time on the vertical axis (h). The color range represents the increase in percentage of cell death of the agent combination as compared to cell death induced by a single agent (values above 20% are red; negative values are blue). **Supplemental Figure 11c** shows that, for the first patient, bortezomib combined with panobinostat (HDACi), had a significant increase in cell-kill as compared to bortezomib alone at all concentrations, with highest benefit in the lowest concentrations. The benefit of bortezomib plus panobinostat relative to single agent panobinostat is restricted mainly to the lowest concentrations. The lowest panel of **Supplemental Figure 11c** depicts the regions of synergy or the area in which the cell-kill of the combination of bortezomib and panobinostat is higher than the Bliss additive[1] effect of both drugs. Similar data for the second patient are presented in **Supplemental Figure 11d** and illustrate the response pattern of CRM1i plus doxorubicin. Synergy between bortezomib and panobinostat[2] as well as CRM1i and doxorubicin[3] have been previously identified, but the graphs from **Supplemental Figures 11c** and **11d** show evidence of how these positive interactions can be limited to a small range of concentrations and narrow windows of time. As such, it appears that synergy is difficult to identify and interpret by classical methods[4,5]. This is especially true for primary cells, where the number of experimental conditions that can be tested in a single sample is limited.

To study drug interactions in patient samples, we have added two drugs at maximum concentration and diluted them serially, so that their concentration ratio remains the same across all wells tested. To assess the benefit of adding panobinostat to a bortezomib regimen for a particular patient, we have subtracted the dose response surface of bortezomib from the dose response surface of the combination. The result is depicted in **Supplemental Figure 11c**, top panel, showing in red the conditions (concentration and exposure time) where the difference in cell kill is higher than 20%. Regions where the increase in cell kill is negligible or negative are shown in blue, and a color gradient is used for the intermediate values. Here we use the classic definition of synergy, which determines that two drugs are synergistic if their combined effect (percent cells killed) is higher than the combination of their independent effect[1]. For instance, consider that drugs A and B, at a specific concentration and during a certain period of time, kill the fractions $a$ and $b$ of cells, where $a<1$ and $b<1$. Should the combination of both drugs kill a fraction equal to $[1-(1-a)*(1-b)]$, then A and B are additive. If the fraction killed is higher, the drugs are synergistic; if lower, they are antagonistic.

***Determination of variation of ex vivo chemosensitivity between sequential samples (test-retest).*** One of the most important components of this assay is the capture of changes in a patient's clinical response over time (sequential therapy). First, we have performed a test-retest in order to assess the inter-day variability of the assay. This variability includes, but is not limited to: inter-day variation of media and reagents, biopsy procedure, MM cell enrichment, plate seeding and drugging with robotic plate handler, sequential imaging, and digital image analysis. **Supplemental Figure 13a** depicts the clinical history of a MM patient who had two biopsies performed within one month, in absence of treatment. We have quantified the chemosensitivity of both biopsies and used this information to build mathematical models of clinical response (red dashed line for

data from biopsy 1, blue solid line for data from biopsy 2) to the therapy the patient ultimately received after the second biopsy (CRM1i + liposomal doxorubicin). Results indicated high correlation between both modeled curves (Pearson r=0.9707) demonstrating reproducibility of the assay, as well as accuracy of predicted depth of response and actual outcome (solid green line). **Supplemental Figure 13b** represents a measure of the inter-day variability of this assay, which is the predicted best clinical response through 90 days, demonstrating inter-day consistency of model predictions.

We also evaluated the influence of therapy on *ex vivo* drug sensitivity in sequential biopsy analyses. **Supplemental Figure 13c** represents a patient with two sequential biopsies separated by five months (**Pt32**). During the intervening period, the patient was treated with a combination of a hypoxia-activated alkylating agent (TH-302), proteasome inhibitor (bortezomib) and immunomodulatory agent (dexamethasone), leading to a partial response followed by relapse. The clinical predictions generated by the mathematical model based on the first biopsy (pre-treatment) indicated that this patient was highly sensitive to bortezomib and melphalan, moderately sensitive to CRM1i, and refractory to liposomal doxorubicin (**Supplemental Figure 13d**). The mathematical models parameterized by the biopsy post-relapse indeed confirm that the tumor has become refractory to bortezomib, maintained its resistance to liposomal doxorubicin, and would present only a minor response to melphalan or CRM1 inhibitor. These data demonstrate the ability of the *ex vivo* model to account for the changing drug resistant subpopulations associated with intervening therapy suggesting that this platform has the potential to provide meaningful information as a clinical decision support tool throughout the course of a patient's cycles of clinical management.

***Determination of intra-plate variation.*** We have characterized the behavior of this assay towards intra-plate variability. It is well known that temperature and gas gradients contribute to location bias in multi-well plates. In order to determine the degree of intra-plate variation or possible spatial bias, we plated primary MM cells from one patient (Pt48, **Supplemental Figure 14**) in co-culture with patient-derived stroma embedded in collagen matrix and repeated a pattern of 3 drugs (melphalan, bortezomib and carfilzomib) as well as negative control, eight times across the plate. Each drug was tested in five different concentrations and two replicates. There were also positive controls for each drug (cell lines at highest concentration, two replicates). We have grouped the measurements of both replicates of each concentration for each drug in each of the eight repeats across the plate. Similarly, we have also grouped and determined the variation in the negative and positive controls. In order to determine the contribution of location in the plate versus exposure time, we have calculated a two-way ANOVA on each combination of drug-concentration (total of 16 ANOVAs). For the control and low concentrations, where there is no measurable drug-induced cell death, the contribution of both exposure time and location in plate should be similar, and the total variation should be negligible. However, for higher drug concentrations, we expected most of the variation to come from exposure time and only a negligible amount to be attributed to location in the plate. In the control wells, 41% of the variation came from exposure time and 36% from location. For the highest concentrations of bortezomib, carfilzomib and melphalan, these values were 99%, 98% and 97% for exposure time, <1%, 2% and 2% for location. Also, as expected, the total variation, quantified as the total sum of squares (SS) in the highest concentrations for bortezomib, carfilzomib and melphalan, were 58-, 50- and 39-fold higher than control, respectively. These test-retest studies demonstrate that the assay is robust with low intra-plate variation.

***Convergence of solution for parameters of ex vivo chemosensitivity.*** **Supplemental Figure 15** shows MATLAB's l*sqcurvefit* converge to the parameter estimates as it approaches a minimal value of *SSR* for the four models fitted to the *ex vivo* data for panobinostat. The single population, no distribution model, as referenced in **Supplemental Table 4**, is the model with the smallest AIC value. Even though the "two-population with distribution" is the model with the least SSR, indicating that the benefit in terms of SSR is marginal as compared to adding additional parameters to the model. It can also be observed that all parameters in the single population model quickly converge and stabilize, while both 2-population models show oscillation of parameters, indicating an underdetermined system.

**Supplemental Figure 16** shows MATLAB's l*sqcurvefit* converge to the parameter estimates as it approaches a minimal value of *SSR* for the four population models fitted to the *ex vivo* data for carfilzomib. The best model chosen based on the least AIC is the one with two populations modeled as distributions as shown in **Supplemental Table 5**. Note the considerable reduction in SSR between two population and one population models, as well as the stability of the parameter values after convergence, validating heterogeneity in tumor population.

**Supplemental Figure 17** depicts a comparison between the clinical predictions for Pt103 using the four different models for bortezomib. Notice the similarity in the clinical predictions and the AIC values. This is a case where all the proposed models fit the data sufficiently well and we choose the model with the least AIC. On the other hand, **Supplemental Figure 18** presents a comparison between the clinical predictions for Pt103 using the four models for carfilzomib. Notice the variation in clinical predictions between the models. This is a case where AIC chooses the model that fits the data best (lowest SSR), two populations modeled as distributions. In summary, the choice of the correct, simplest model, may lead to significant differences in the clinical outcome.

***Extended Description of Mathematical Model.*** We propose a nonlinear dynamical model to describe the growth/death of tumor populations in MM patients. For this purpose, we employ a statistical, grey-box, parametric model that represents the tumor's response to various drugs by modeling them as a distribution of populations, where each subpopulation has a different level of sensitivity to a given drug concentration. Further, within a subpopulation it is assumed that the likelihood of cell death depends on the drug concentration.

Let the total number of MM cells in the patient's body be quantified and represented by *p(t)*, which stands for population of tumor cells. The tumor burden, in the absence of treatment, is assumed to increase with time due to cell replication.

The non-monotonic variation of the tumor population was modeled as a difference equation

$$p(t+dt) = p(t)G(dt)D(t,dt), \qquad \text{(Equation S1)}$$

where *G(dt)* is the growth factor due to tumor cell replication and *D(t,dt)* is the death factor due to drug-induced cell death between times *t* and *t+dt*.

*Tumor growth in absence of therapy.* In cell culture, the time required for the number of cells in a flask to double, commonly known as doubling time, is used as a metric for quantifying growth due to cell replication. For mammalian cells this number is often around 24 hours. However, the doubling time of MM tumors is much longer due to its characteristically low proliferative index. In the mathematical model, the growth factor for the MM population in the absence of therapy is:

$$G(dt) = \left(1 + LI\left(2^{\Delta t} - 1\right)\right)^{dt/\Delta t}, \qquad \text{(Equation S2)}$$

where *dt* is a time interval (in days) between measurements, labeling index *LI* is the percentage of MM cells actively replicating, and $\Delta t$ is the time step used during simulation.

Let a given patient have a *LI* of 3% and say we would like to determine the growth of the tumor over a period of three days. Using Equation 2 with a *LI* of 0.03, *dt* of 3 days, and $\Delta t$ of 5 minutes or 1/288 days:

$$G(3) = \left(1 + 0.03\left(2^{1/288} - 1\right)\right)^{3\times 288} = 1.064.$$

Thus, the MM population, or tumor burden, would increase 6.4% in three days for this patient. Conversely, to determine *LI* for a given patient, we use a method similar to the calculation of doubling time in cell culture. We use the two closest prior measures of tumor burden as obtained from monoclonal paraprotein, a surrogate of tumor burden in MM, and use Equations S1 and S2 to determine *LI*. For example, prior to the current biopsy, a MM patient had two measures of Serum-free light chain (lambda) confirming relapse, where the first was 996mg/L and the second measure was 1,312mg/L, 34.2 days later. Thus, *LI* can be calculated as:

$$LI = \frac{\left(\frac{p(t+dt)}{p(t)}\right)^{\Delta t/dt} - 1}{\left(2^{\Delta t} - 1\right)} = \frac{\left(1312/996\right)^{1/(288\times 34.2)} - 1}{\left(2^{1/288} - 1\right)} = 0.0116, \text{ or } 1.16\%.$$

*Therapy-induced death of tumor cells.* Prior to modeling the stochastic cell death process, we have proposed an empirical pharmacodynamics model based on the drug occupancy theory, described by the reaction [6]

$$\left[\text{Drug}\right] + \left[\text{Receptor}\right] \underset{\text{Dissociation}}{\overset{\text{Binding}}{\rightleftharpoons}} \left[\begin{array}{c}\text{Drug-Receptor}\\ \text{Complex}\end{array}\right] \xrightarrow{\text{Threshold}} \text{Response},$$

where drug and receptor molecules form drug-receptor complexes, which in turn cause cellular damage and, beyond a certain threshold, initiates cell death. The dynamics of this reversible reaction follows

$$\frac{d\beta}{dt} = \underbrace{-\kappa\,\beta(t)}_{\text{Dissociation}} + \underbrace{\delta\,R(t)^h}_{\text{Binding}},$$

(Equation S3)

where, the forward rate of reaction is given by the law of mass action [7] and is described as the rate of binding alone

$$\left.\frac{d\beta}{dt}\right|_f = \left(K_f\left[\text{Receptor}\right]^s\right)R(t)^h = \delta\,R(t)^h,$$

(Equation S4)

where, *R(t)* is the drug concentration at time *t*. *s* and *h* are stoichiometric coefficients of the reversible reaction. Further the rate of dissociation is proportional to the extent of binding $\beta(t)$ and and an empirical rate constant $\kappa$. Equation S3 is in Bernoulli's ODE form and has an analytical solution assuming binding starts at t=0.

$$\beta(t) = \delta\int_0^t e^{-\kappa(t-T)}R(T)^h dT,$$

(Equation S5)

When the cellular damage is greater than the threshold, the probability of cell death increases asymptotically with increase in damage as in a sigmoid function

$$y(x) = 1 - \frac{1}{1+e^{-\sigma x}},$$

(Equation S6)

Where *e* is the Euler's number and $\sigma$ is a positive number defining the steepness of the curve. As the probability of cell death cannot be negative, Equation S6 was modified such that the death function *D* varies from 1 to 0.5 as the accumulated binding beyond the threshold varies from 0 to $\infty$:

$$D(t,dt) = 1 - 0.5\tanh\left(\alpha(t)/2\right)dt,$$

(Equation S7)

$$\alpha(t,dt) = \max\left(\frac{\beta(t,dt)-\tau}{\delta}, 0\right)$$

(Equation S8)

where $\alpha$ is a measure of accumulated damage beyond the threshold, $\tau$, and $\delta$ is a non-dimensionalizing empirical factor.

*Modeling heterogeneity in tumor population.* The short-term response of MM patients to therapy can be monotonic (continuous increase or decrease of tumor burden), or may present an inflexion point followed by relapse (**Figure 2a-c**). Thus, the tumor chemosensitivity of MM patients cannot always be accurately described by a single "clonal" population, but requires a more general representation. In this model, we propose the tumor composed of two subpopulations, with different degrees of sensitivity to therapy. Each subpopulation

can either be modeled as "clonal" or as a distribution, with drug-specific threshold values ($\tau$, Equation S8). These threshold values are obtained from a normally distributed probability density function (defined in terms of a drug-specific mean and variance) that specifies the fraction of a subpopulation that initiates cell death beyond a given threshold. The rationale behind adopting such an approach lies in the assumption that both sensitive and resistant subpopulations have their own degree of heterogeneity. **Figure 2b** shows an example of such a representation of tumor chemosensitivity as a single and as a double distribution.
The total tumor burden of a patient is

$$p(t+dt) = \sum_{j=1}^{2} p_j(t+dt), \quad j = 1,2 \text{ subpopulations}, \qquad \text{(Equation S9)}$$

where the composition of each subpopulation at initial time $t_0$ is modeled as a distribution

$$PDF\left(\tau; \mu_j, {\sigma_j}^2\right) = \frac{1}{\sqrt{2\pi {\sigma_j}^2}} \exp\left( -\frac{\left(\tau - \mu_j\right)^2}{{\sigma_j}^2} \right) \qquad \text{(Equation S10)}$$

with a specific mean $\mu_j$ and standard deviation $\sigma_j$ that define the percentage of cells that initiate cell death when the accumulated damage surpasses $\tau$. For computational purposes, we have discretized this distribution in a histogram with *n* bins, ranging from $\mu_j - 6\sigma_j$ to $\mu_j + 6\sigma_j$, using MATLAB's function *normpdf* (**Supplemental Figure 2**).

$$p_{j,i}(t+dt) = p_{j,i}(t) G(dt) D_j(t, dt, \tau_i), \quad j = 1,2 \text{ subpoplations. } i = 1,\ldots,n \text{ bins.} \qquad \text{(Equation S11)}$$

$$p_j(t+dt) = \sum_{i=1}^{n} p_{j,i}(t+dt), \quad j = 1,2 \text{ subpopulations. } i = 1,\ldots,n \text{ bins.} \qquad \text{(Equation S12)}$$

There is no biological meaning for negative $\tau$ values, so the histogram is truncated when $\mu_j - 6\sigma_j < 0$, and the value of each bin is normalized so that the sum of all bins corresponds to $p_j$. Thus, at initial time $t_0$, the composition of the $j^{th}$ subpopulation

$$p_{j,i}(t_0) \approx \frac{\hat{p}_{j,i}(t_0)}{\sum_{i=1}^{n} \hat{p}_{j,i}(t_0)} \times p_j(t_0), \qquad j = 1,2 \text{ subpopulations. } i = 1,\ldots,n \text{ bins}, \qquad \text{(Equation S13)}$$

where $\hat{p}_{j,i}(t_0) = \begin{cases} PDF\left(\tau_i; \mu_j, \sigma_j\right), & \forall \tau_i \geq 0 \\ 0, & \forall \tau_i < 0 \end{cases}$

In summary, the model assumes the existence of two tumor subpopulations, with different degrees of chemosensitivity. Each subpopulation, in turn, exhibits a range of sensitivity to therapy modeled as a normally distributed probability density function. The total number of parameters for this general model is nine: two subpopulation-specific mean and standard deviation, two reaction constants $\delta$, one drug-specific cell repair rate $\kappa$, one drug-specific empirical parameter *h* relating drug concentration to response, and the ratio of sensitive population to the entire tumor population.

In specific cases, the estimated standard deviation may be so small that it may be beneficial to model one subpopulation as a Dirac delta function. In such a case, the threshold $\tau$ could be estimated directly, reducing the total number of parameters of the system to seven. Additionally, one of the populations may be so small that its effect cannot be detected by the *ex vivo* assay, and thus the tumor could be modeled as only one population.

*Determining model parameters for a specific drug-patient combination.* Before predicting the clinical response of MM patients using the proposed model, we need to, firstly, estimate the parameters for all the models specified above using *ex vivo* data, and secondly, choose the model that best fits the data. One of the challenges faced in dealing with *ex vivo* data is to ensure that it best represents tumor response *in vivo*. An

important point in this process is to differentiate between drug-induced cell death, *D(t,dt)* in Equation 1, and spontaneous *ex vivo* cell death. This is accomplished by normalizing the *ex vivo* response of the tumor to a specific concentration of a drug with the *ex vivo* vehicle control. Let

$$p_{R_x}(t+dt) = \left( p_{R_x}(t) D_e(t,dt) \right) G(dt) D(t,dt) \quad \text{(Equation S14)}$$

represent the response of tumor to drug $R_x$ *ex vivo*, where $D_e(t,dt)$ represents the rate of spontaneous cell death. Further, let

$$p_c(t+dt) = p_c(t) G(dt) D_e(t,dt) \quad \text{(Equation S15)}$$

represent the *ex vivo* behavior of the control. By dividing Equations S14 and S15, we have

$$\frac{p_{R_x}(t+dt)}{p_c(t+dt)} = \left( \frac{p_{R_x}(t)}{p_c(t)} \right) D(t,dt), \quad \text{(Equation S16)}$$

where $\frac{p_{R_x}(t+dt)}{p_c(t+dt)}$ and $\frac{p_{R_x}(t)}{p_c(t)}$ represent *p(t+dt)* and *p(t)* respectively, in Equation S1. Thus, by dividing every *ex vivo* response curve by the corresponding vehicle control we are able to discard *ex vivo* spontaneous cell death and quantify direct drug-induced cell death. The parameters can then be estimated using MATLAB's *lsqcurvefit*, which minimizes the sum of squares of the residual (difference between normalized *ex vivo* data and the model estimate) at every data point. The *ex vivo* data consists of percent live cells normalized by control at 0 hours, drug concentration, and exposure time. Our objective is to estimate the set of parameters that best fit this data using the least squares method. Further, we used Akaike Information Criterion[8] (AIC)

$$AIC = 2k + n \ln\left( SSR / n \right), \quad \text{(Equation S17)}$$

where SSR is the sum of squares of residual, n is the number of data points used for estimation, and k is the total number of parameters used to describe the model. The model with the smallest AIC is considered to be the best model.

**Supplemental Figures and Tables:**

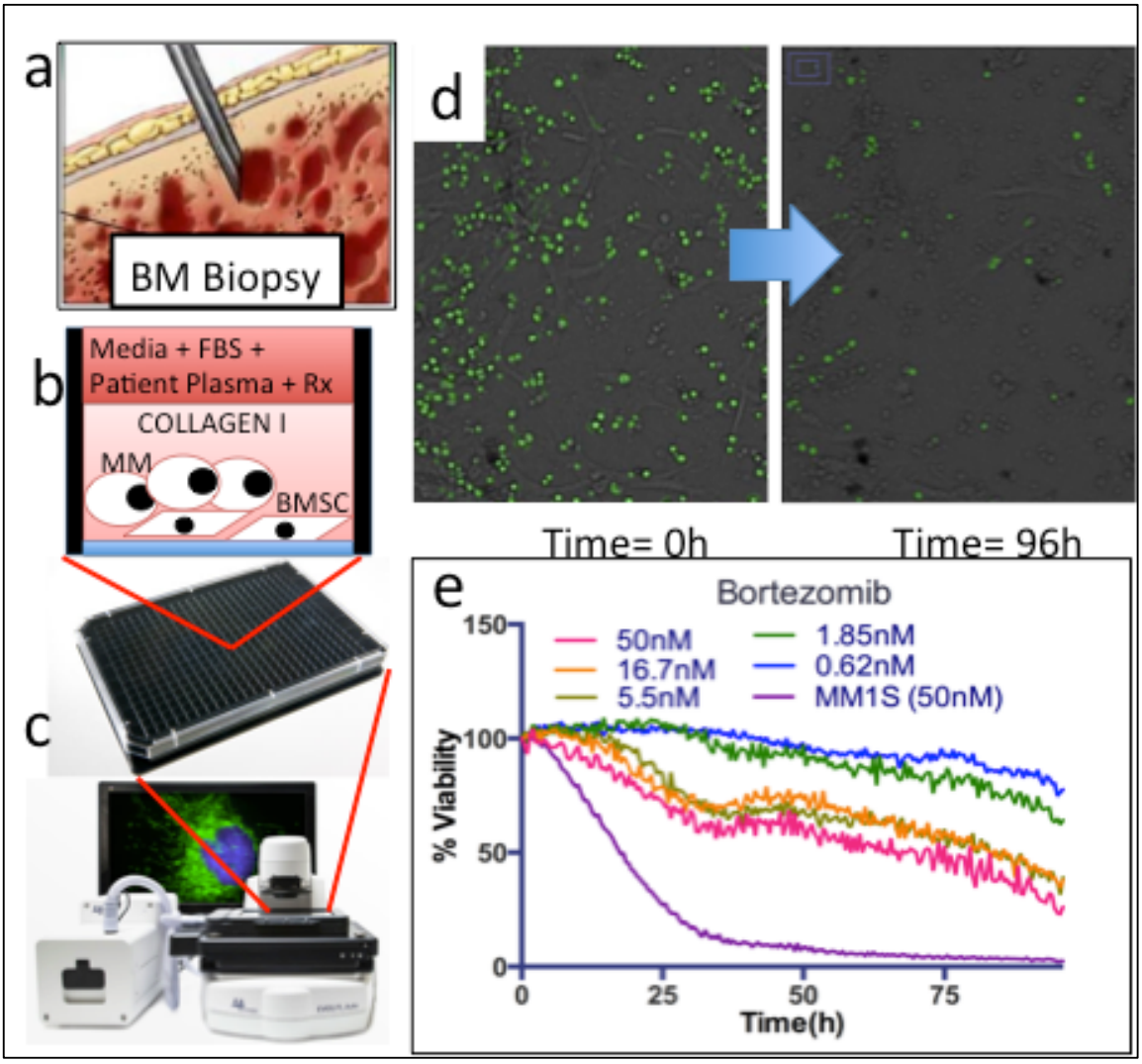


**Supplemental Figure 1. Overall workflow of ex vivo chemosensitivity assay.** During a standard-of-care bone marrow biopsy myeloma cells are separated from non-cancer by CD138-positive magnetic bead sorting. (a) Cancer cells are re-suspended in collagen-I in conjunction with stroma (adherent non-cancer cells obtained from bone marrow biopsies, CD138-). (b) The cell-matrix mix is seeded in a multi-well plate and left to polymerize overnight. Wells are organized so that 31 drugs can be tested at 5 different concentrations with 2 replicates. (c) By imaging at regular intervals each well in bright field, and using a digital image analysis algorithm, we non-destructively detect live and dead cells (d). (e) Digital image analysis algorithm quantifies longitudinal changes in number of live MM cells in each well and generates dose-response curves for each of the five concentrations plus the positive control (cell line MM1.S under highest concentration only).

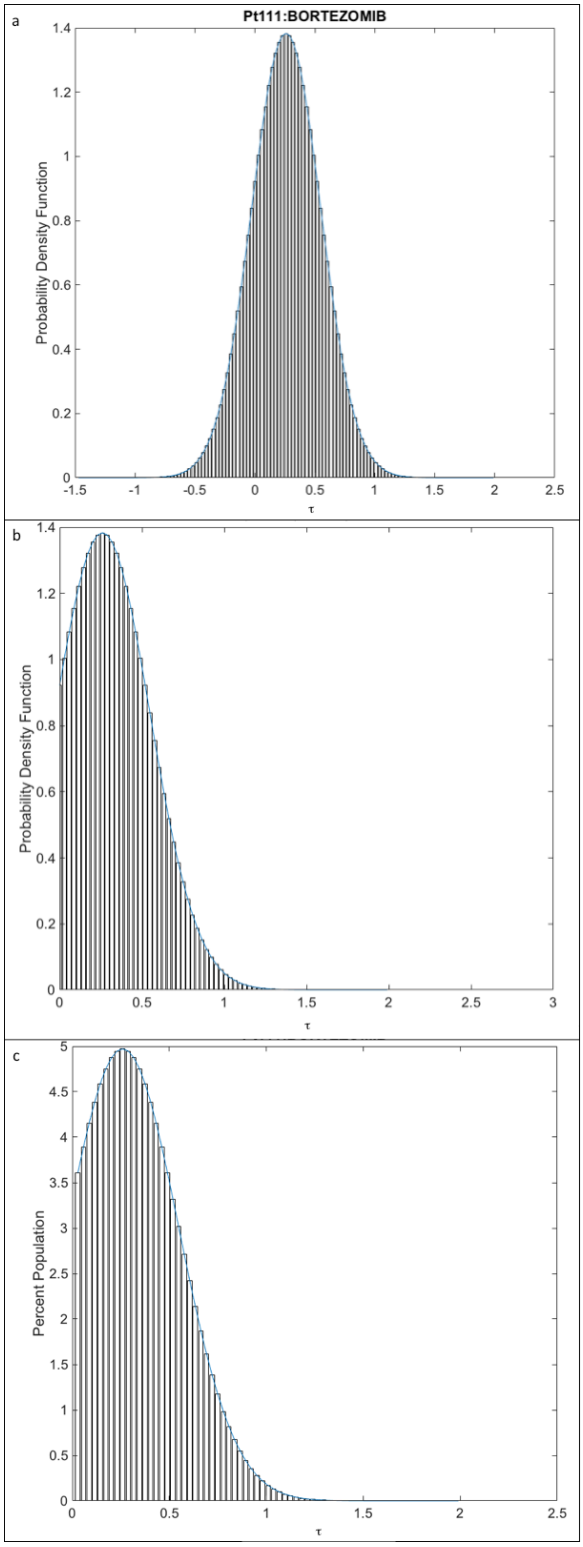


**Supplemental Figure 2. Computational implementation of tumor sensitivity as a probability distribution.** In the example above, patient Pt111's bortezomib sensitivity was best represented as a single mode normal distribution with regards to the threshold variable t. The distribution was approximated to a histogram spanning 12 standard deviations, with 10 bins per standard deviation (**a**). Since t is a positive value, the distribution is truncated to remove negative values for t (**b**). To ensure that the sum of all bins amounts to 100%, we multiply each bin by the sum of all bin values and multiply by 100% (**c**).

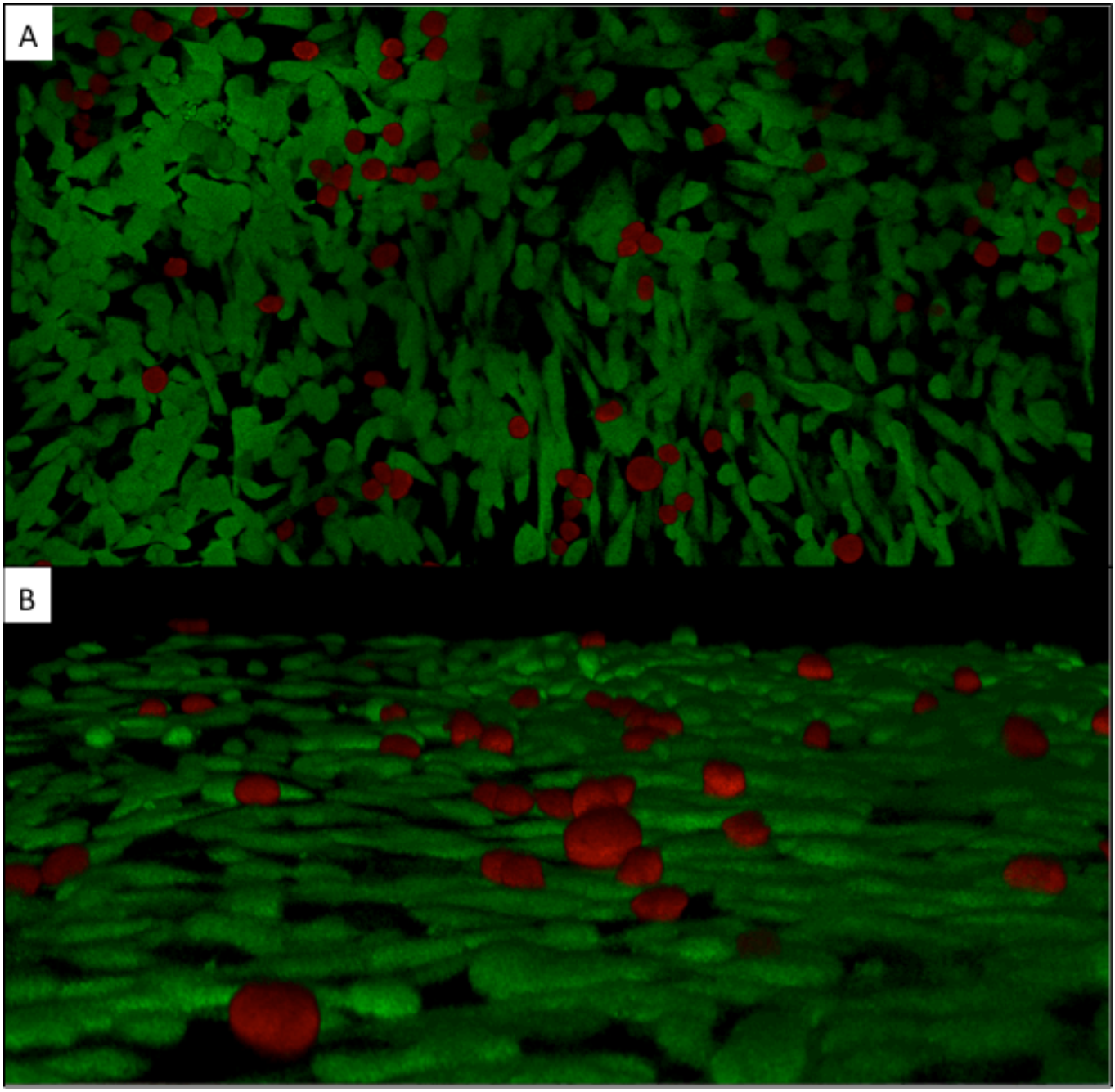


**Supplemental Figure 3. Spatial co-localization of MM and stroma.** Confocal microscopy of co-culture of stably transfected human myeloma cell line 8226/dsRed2 and human stromal cell line HS-5/GFP confirm that MM cells maintain a round shape while stroma stretches and adheres to bottom of well (A) while both populations maintain close contact and adhesion (B).

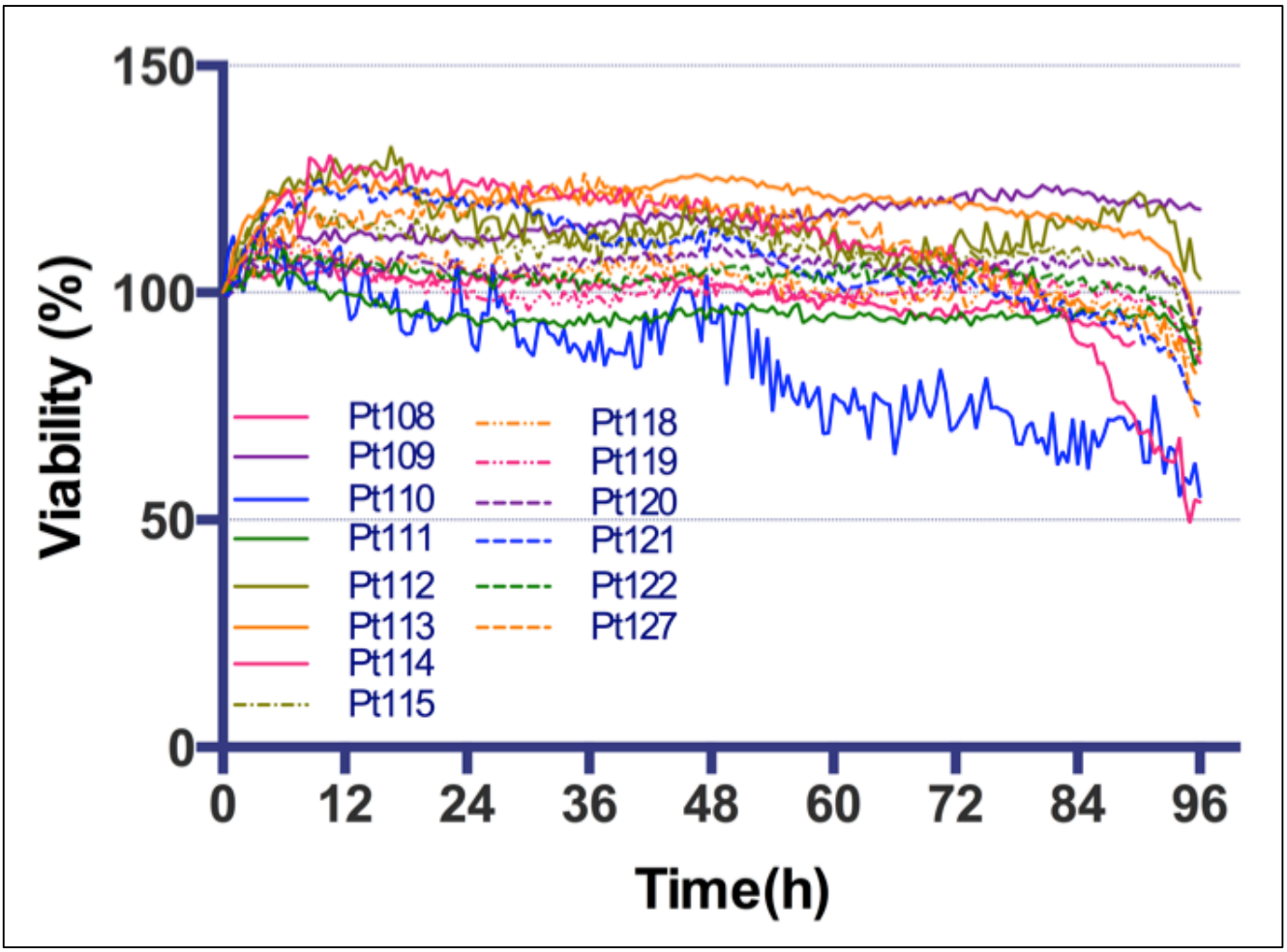


**Supplemental Figure 4. Example of assessment of spontaneous cell death in 14 primary MM samples across 96h in EMMA's ex vivo assay.** Please note the border effect artifact that suggests increase in viability in the beginning of the experiment, and decrease at the end. This border effect is removed when the curves from each experimental condition is divided by the corresponding controls. In the examples above, only the samples from patients Pt108 and Pt110 had a significant rate of spontaneous cell death, while the remaining patients had less than 25% loss of viability under control conditions.

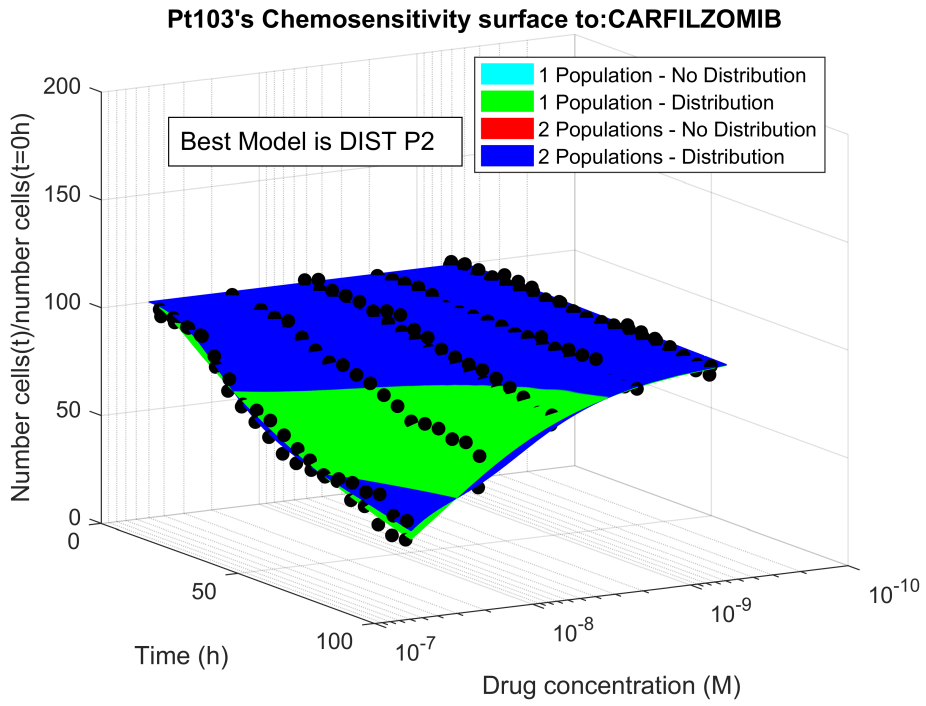


**Supplemental Figure 5. Ex vivo chemosensitivity curve of patient Pt103 to carfilzomib.**

| Parameter | Obtained from | Used in | Value |
|---|---|---|---|
| $LI$ | Previous relapse or 1% if naïve | Eq. (S3) | 1.44% |
| $a_1, \mu_1$ | Ex vivo assay | Eq. (S10) | 8.0139e-3 |
| $a_2, \delta_1$ | Ex vivo assay | Eq. (S9) | 7.3421e-4 |
| $a_3, \kappa$ | Ex vivo assay | Eq. (S4) | 0.012432 |
| $a_4, h$ | Ex vivo assay | Eq. (S4) | 0.4669 |
| $a_5, \sigma_1$ | Ex vivo assay | Eq. (S10) | 4.007e-3 |
| $a_6, p_1$ | Ex vivo assay | Eq. (S14) | 47.098% |
| $a_7, \mu_2$ | Ex vivo assay | Eq. (S10) | 0.024996 |
| $a_8, \sigma_2$ | Ex vivo assay | Eq. (S10) | 6.3511e-3 |
| $a_9, \delta_2$ | Ex vivo assay | Eq. (S9) | 5.4014e-4 |

**Supplemental Table 1. Model parameters for patient Pt103's primary MM cells tested ex vivo with carfilzomib.**

**Supplemental Figure 6. Correlation between predicted trajectories and actual clinical response of 52 MM patients up to 90 days post biopsy.**
Please see document with 52 pages, one for each patient.

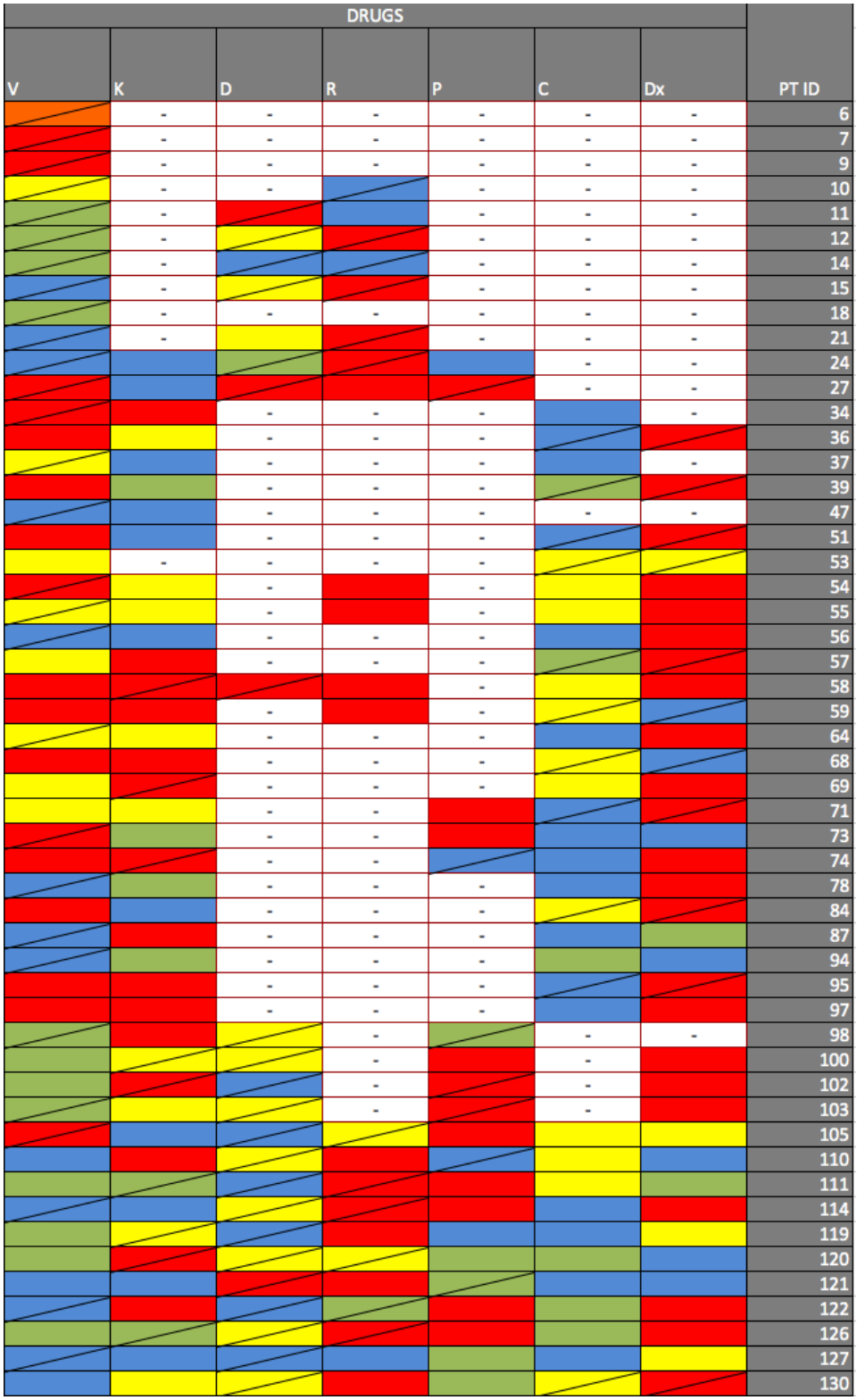


**Supplemental Table 2. Choice of best therapeutic option based on EMMA.** The above table groups the clinical predictions of the 52 MM patients in this study for 7 individual drugs: bortezomib (V), carfilzomib (K), dexamethasone (D), lenalidomide (R), pomalidomide (P), CRM1i (C) and doxorubicin (Dx). Each prediction is color coded as follows: green for VGPR/CR, orange for MR/PR, yellow for SD, and red for PD. Drugs that were not tested *ex vivo* for a patient sample appear as white. Diagonal lines mark the drugs that were actually administered to the patients. This dataset suggests that approximately 40% of the agents administered to these patients had no clinical efficacy (diagonal marked red cells). In addition, the model predictions suggested a different therapeutic choice, with deeper response, for 16 patients (27, 34, 37, 64, 69, 73, 78, 84, 87, 94, 100, 102, 119, 120, 127 and 130).

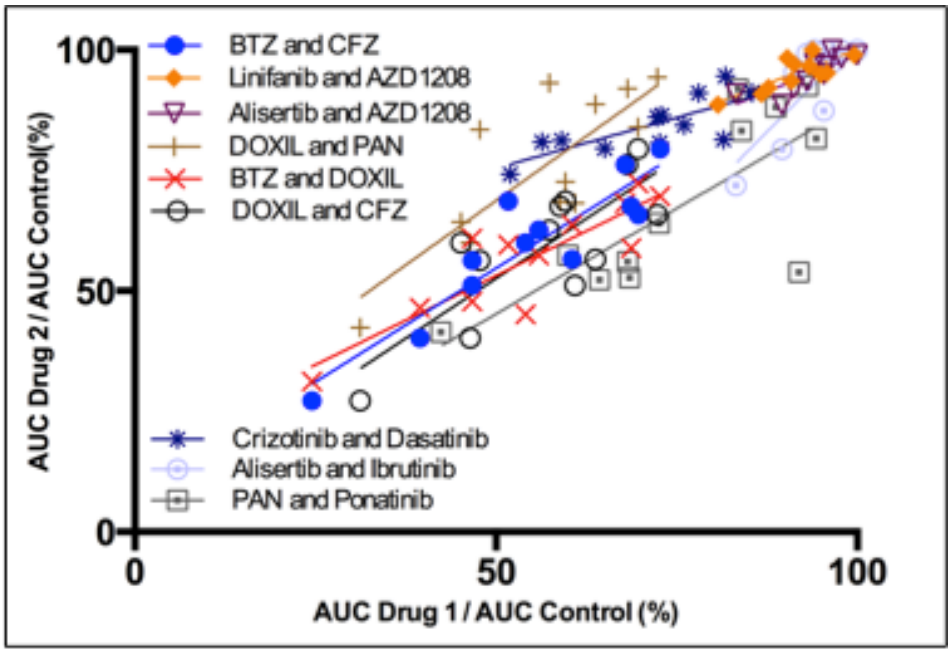


**Supplemental Figure 7. Correlation between *ex vivo* drug efficacy in 12 MM patients tested with six chemotherapeutic agents and 25 PKIs.** We have paired the 31 agents and calculated the linear regression of area under the curve (AUC) across 12 MM patients in order to determine correlation of drug sensitivity. The top correlations are depicted in the figure: bortezomib and carfilzomib (Pearson r=0.9141), bortezomib and doxorubicin (r=0.8762), linifanib and azd1208 (r=0.8322), doxorubicin and carfilzomib (r=0.8136), doxorubicin and panobinostat (r=0.8046), crizotinib and dasatinib (r=0.7764), alisertib and azd1208 (r=0.7752), alisertib and Ibrutinib (r=0.7749) and panobinostat and ponatinib (r=0.7694).

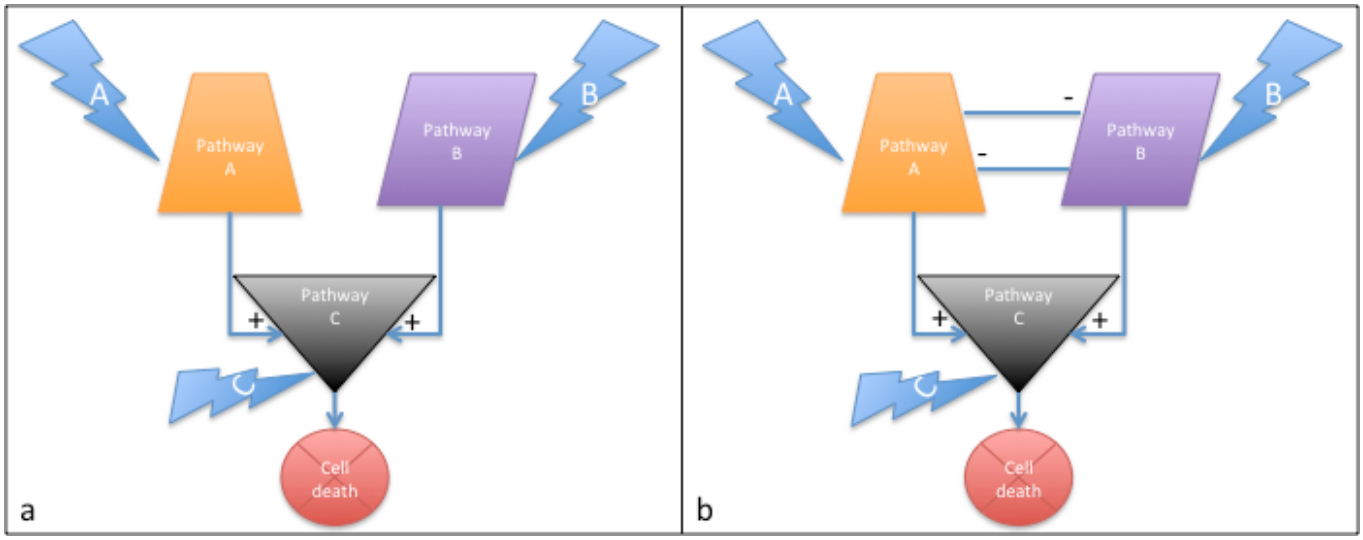


**Supplemental Figure 8. Hypothetical models for inter-patient correlation of drug sensitivity.** (**a**) Consider two independent pathways, A and B, converging downstream into pathway C. Drugs that target any of these pathways can cause cell death. Cellular adaptations that downregulate pathway C will make the cell resistant to drugs that target this pathway and also cross-resistant to those upstream (A and B). In other words, resistance to drugs that target pathway C will correlate with resistance to drugs that target either A or B, and vice versa. While (**a**) is a common motif in intracellular cell signaling, and explains the commonly observed development of cross-resistance observed in patients in the clinic, the explanation of cross-sensitivity, or increase in sensitivity to one drug as a consequence of increase in resistance to another, requires a more complex motif (**b**). In this network, once again pathway C is downstream from A and B, but now pathways A and B suppress each other. Thus, mutations that downregulate the effect of pathway A will cause upregulation of pathway B and thus increase in sensitivity to drugs targeting pathway B. This is a less common motif and possibly explains the lack of drugs with negative correlation of sensitivity in the panel of 25 PKIs studied in this work.

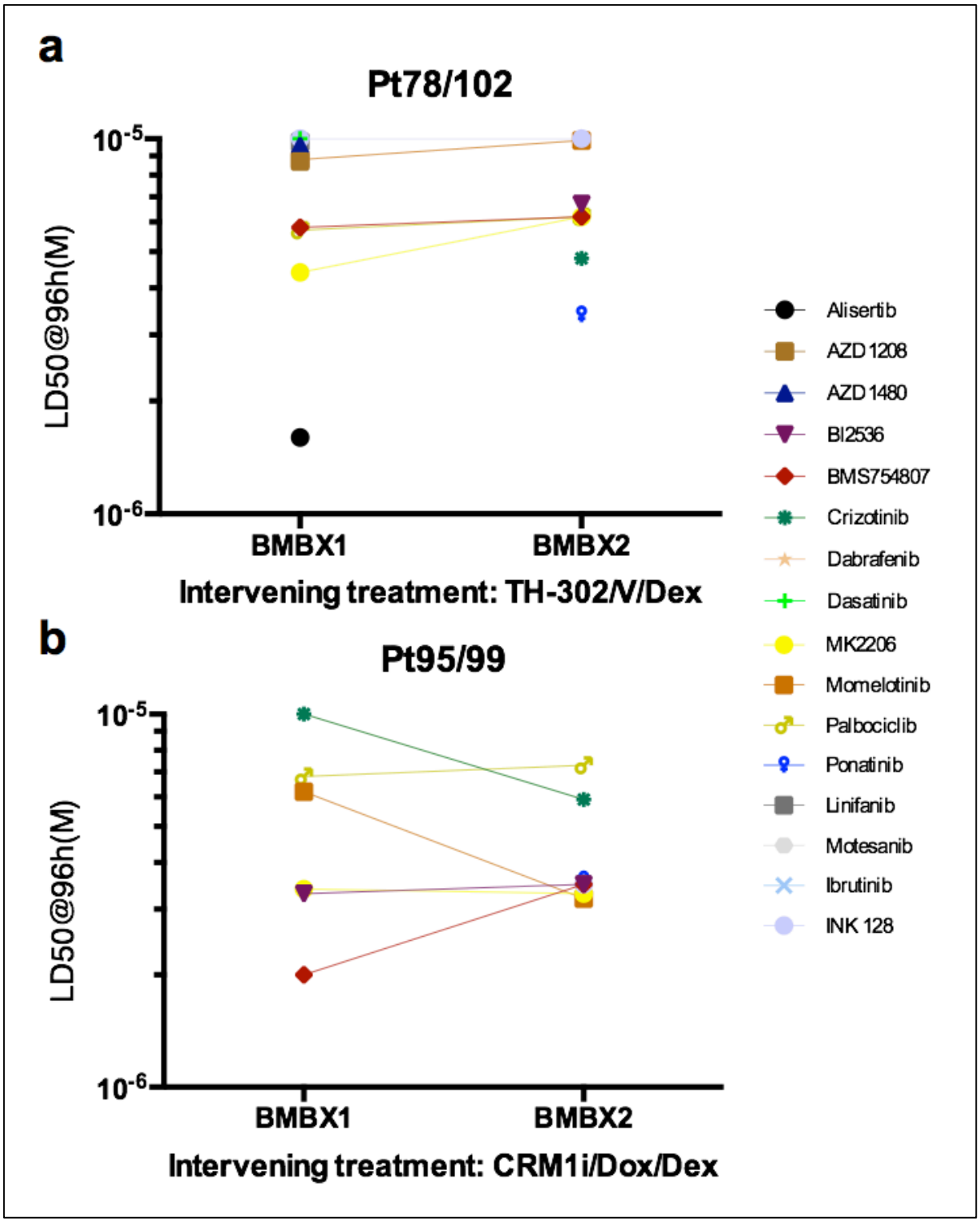


**Supplemental Figure 9. Changes in chemosensitivity of tumor cells from two MM patients to 20 PKIs between two sequential biopsies.** Each marker represents the LD50 at 96h for a particular combination of patients/biopsy. When LD50 is not reached, the marker is absent. For 4 PKIs (Ruxolitinib, Selumetinib, Tozasertib and Trametinib), the LD50 at 96h was higher than me maximum concentration tested (10μM) and thus could not be determined. (a) This patient provided two biopsies separated by an interval of 4 months, during which the patient was treated with a combination of the hypoxic pro-drug TH-302, bortezomib and dexamethasone. Some PKIs were more effective in the first biopsy than in the second (e.g. Alisertib and Dasatinib) while others only more efective in the second biopsy (e.g. Ponatinib, Crizotinib and BI2536). (b) This patient provided two biopsies separated by three weeks, during which the patient was treated with the nuclear export inhibitor selinexor, liposomal doxorubicin and dexamethasone. The most noticeable increases of sensitivity were Crizotinib and Momelotinib, and the most noticeable increase in resistance was BMS754807.

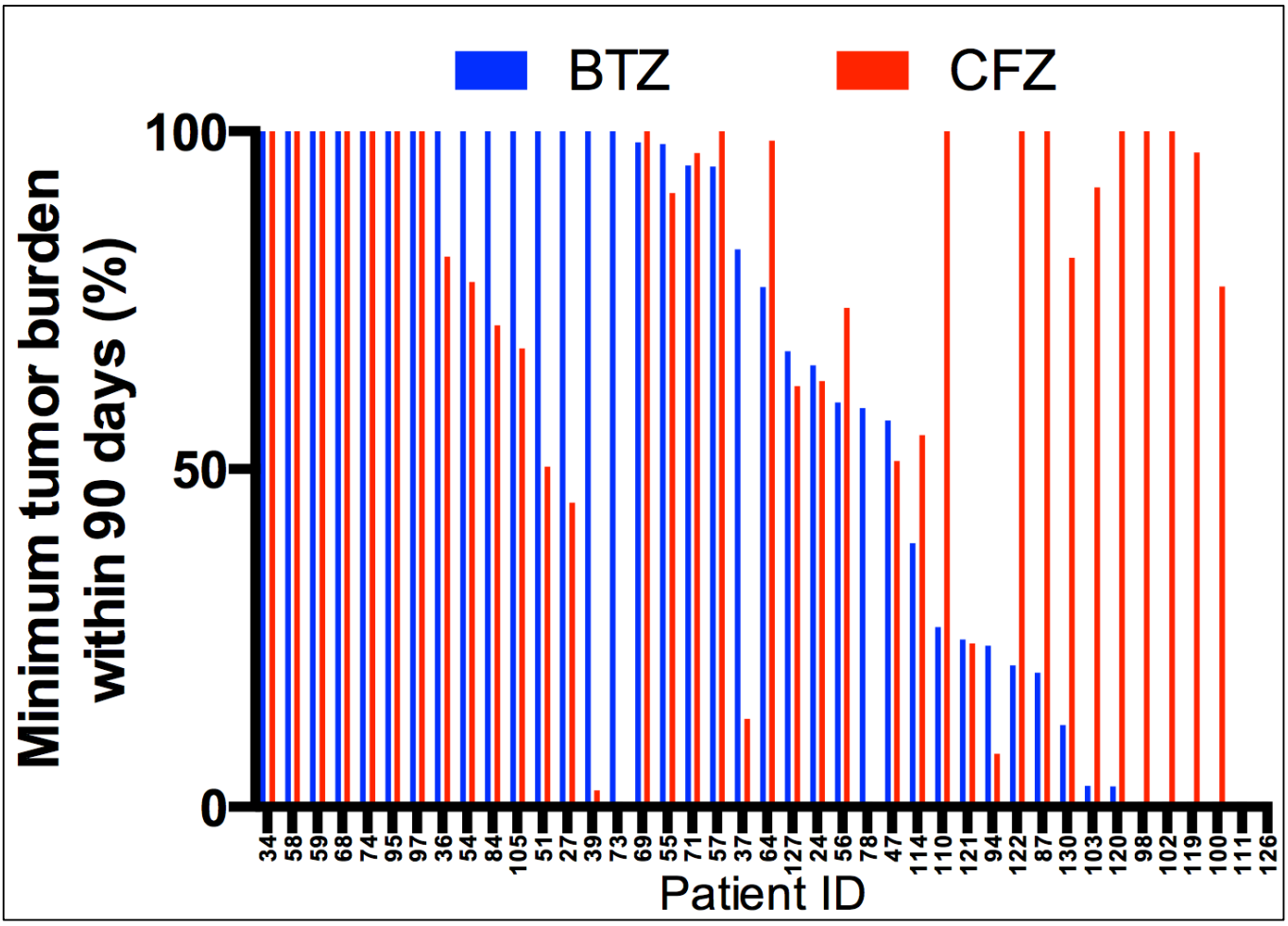


**Supplemental Figure 10. Model predictions of 41 MM patients indicate no correlation between bortezomib and carfilzomib 90-day depth of response.** For each patient, the blue and red lines represent the minimum tumor burden expected in a 90-day treatment with single agent bortezomib and carfilzomib, respectively. Patients have been sorted from left to right in descending order of clinical resistance to bortezomib.

| Patient ID | Status at biopsy | Age | Sex | Race | t(11:14) |
|---|---|---|---|---|---|
| 127 | NDMM | 58 | Female | Black or African American | NO |
| 129 | Triple | 60 | Male | Black or African American | NO |
| 130 | Quad | 76 | Male | White | NO |
| 135 | Naïve | 70 | Female | White | NO |
| 138 | Naïve | 60 | Male | White | NO |
| 140 | NDMM | 68 | Male | White | YES |
| 141 | PI-R | 62 | Male | White | NO |
| 142 | NDMM | 75 | Male | White | YES |
| 143 | PI-R | 66 | Female | White | NO |
| 144 | Naïve | 69 | Female | White | NO |
| 145 | Double | 55 | Female | White | NO |
| 148 | Triple | 54 | Female | White | YES |
| 152 | NDMM | 69 | Male | White | NO |
| 160 | NDMM | 45 | Male | White | NO |
| 161 | Naïve | 60 | Male | White | YES |
| 163 | Double | 73 | Female | White | NO |
| 164 | Triple | 52 | Male | Other | NO |
| 165 | Naïve | 68 | Male | White | NO |
| 166 | Penta | 69 | Female | White | YES |

**Supplemental Table 3. Demographics of patients whose bone marrow aspirates were used in virtual clinical trials of ricolinostat and venetoclax.** Status at bone marrow biopsy were: newly diagnosed (NDMM), proteasome inhibitor resistant (PI-R), double-refractory, triple-refractory, quad-refractory, penta-refractory, and naïve (relapse in absence of therapy). Patients were also classified according to presence of translocation 11,14 in standard of care MM FISH.

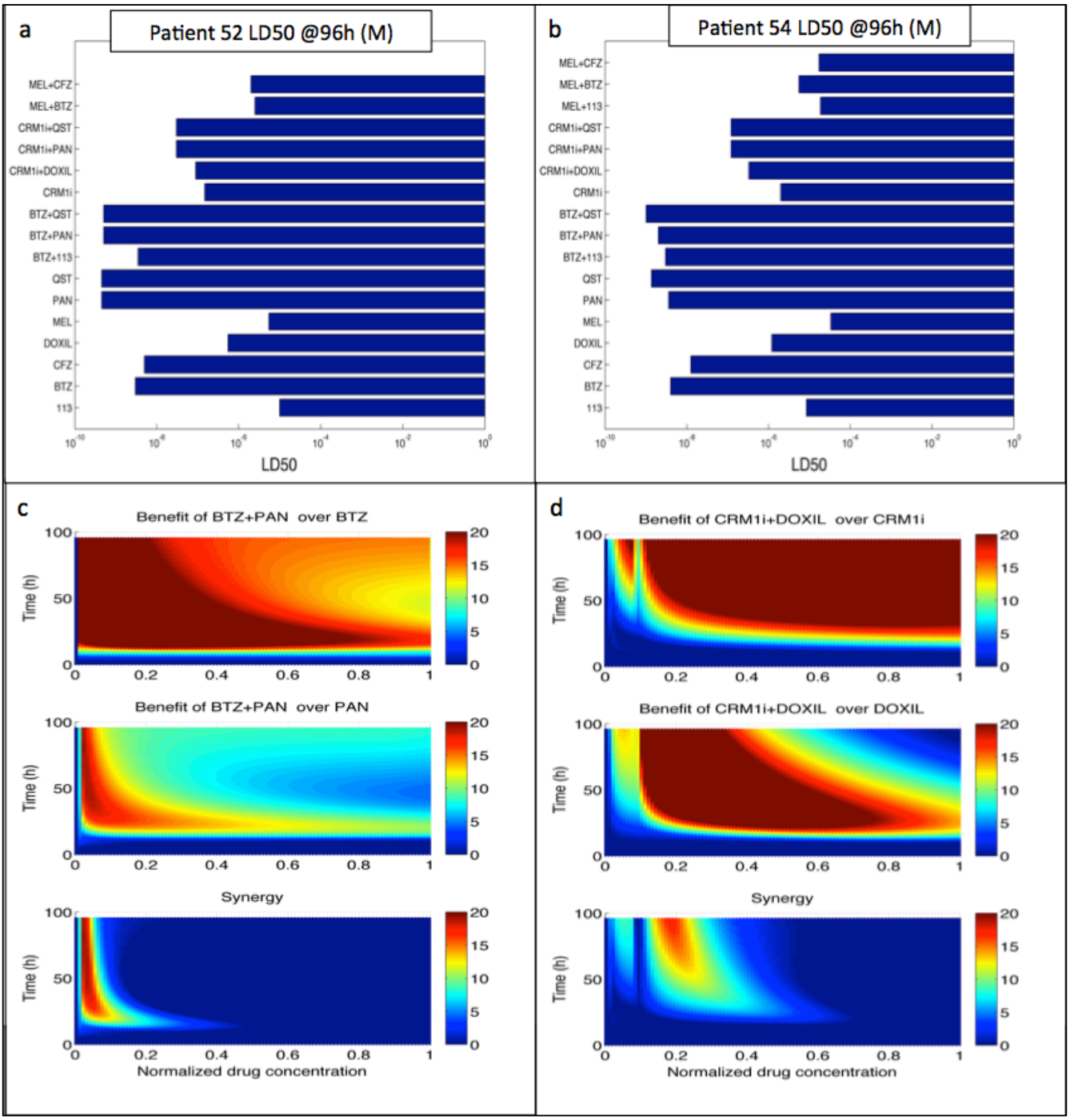


**Supplemental Figure 11. Quantification of drug sensitivity and time-dependent synergy in primary MM cells.** (**a**) and (**b**) represent the LD50 (concentration for 50% reduction in viability as compared to the beginning of experiment, normalized by control) of primary MM cells from two patients. Please note that for drug combinations, only the LD50 of the first drug is shown. (**c**) and (**d**) show a more detailed representation of drug efficacy across concentration and exposure time, revealing the concentrations where drug combinations increase cell kill, and identifying possible synergy "islands", where effect of the drug combination is higher than the product of their individual efficacies. List of drugs tested ex vivo: MEL (melphalan), CFZ (carfilzomib), BTZ (bortezomib), CRM1i (selinexor), QST (quisinostat), PAN (panobinostat), DOXIL (liposomal doxorubicin) and 113 (defactinib).

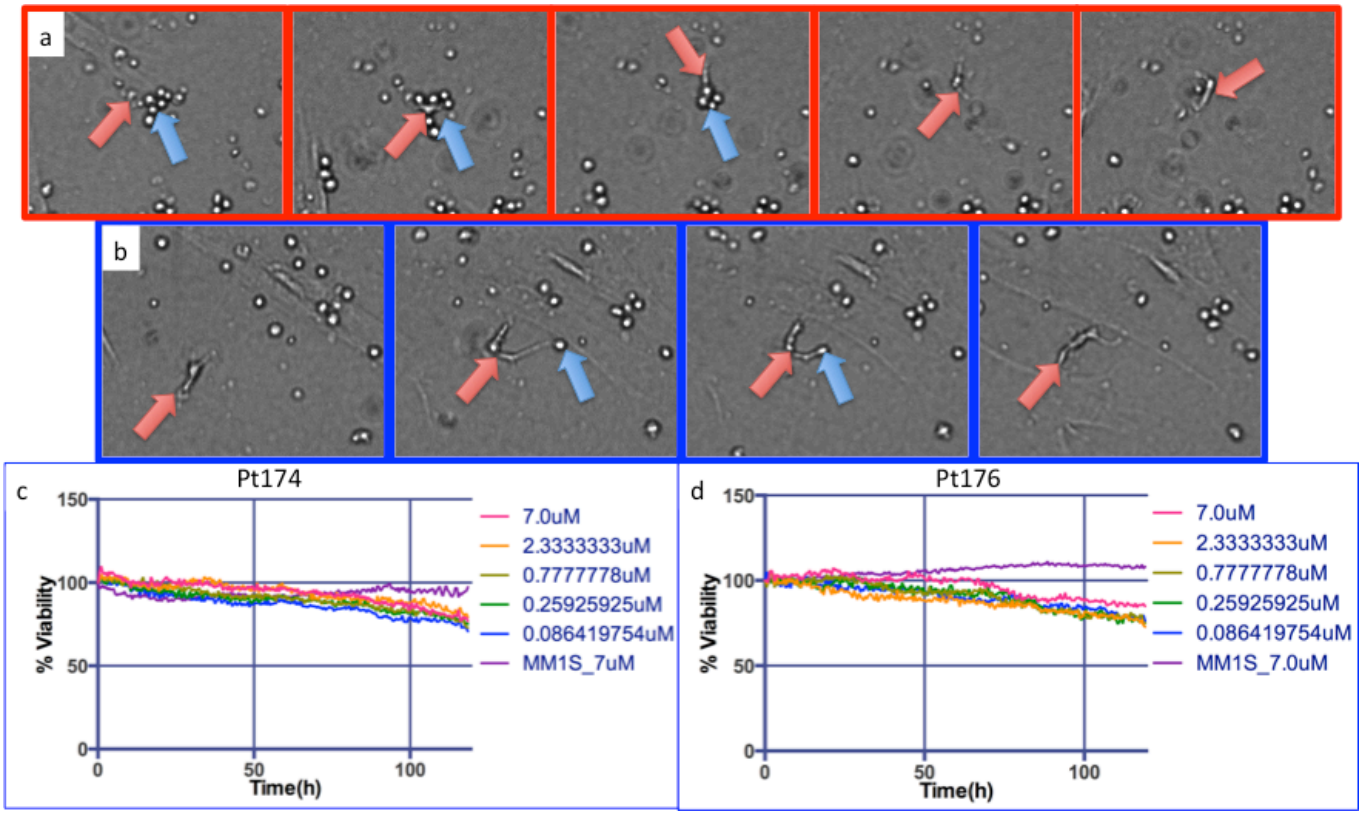


**Supplemental Figure 12. Daratumumab-mediated MM cell death.** Unlike drugs with direct cytotoxic activity studied in this manuscript, daratumumab, a CD38 monoclonal antibody[9,10], mediates immune response to MM cells. The first and second panels (**a** and **b**) depict two separate groups of MM cells from patient Pt174 (blue arrow) during an EMMA assay, exposed to 7μM of daratumumab for 120h. After approximately four days of exposure, a yet-to-be-determined adherent cell (red arrow), originated from either the patient aspirate or stroma, begins to engulf the MM cells in its vicinity, and proceeds to other regions of the well. This process is observed in all wells with daratumumab, from concentrations 7μM to 86nM; it does not occur in controls, and was observed in two separate patients (**c**).

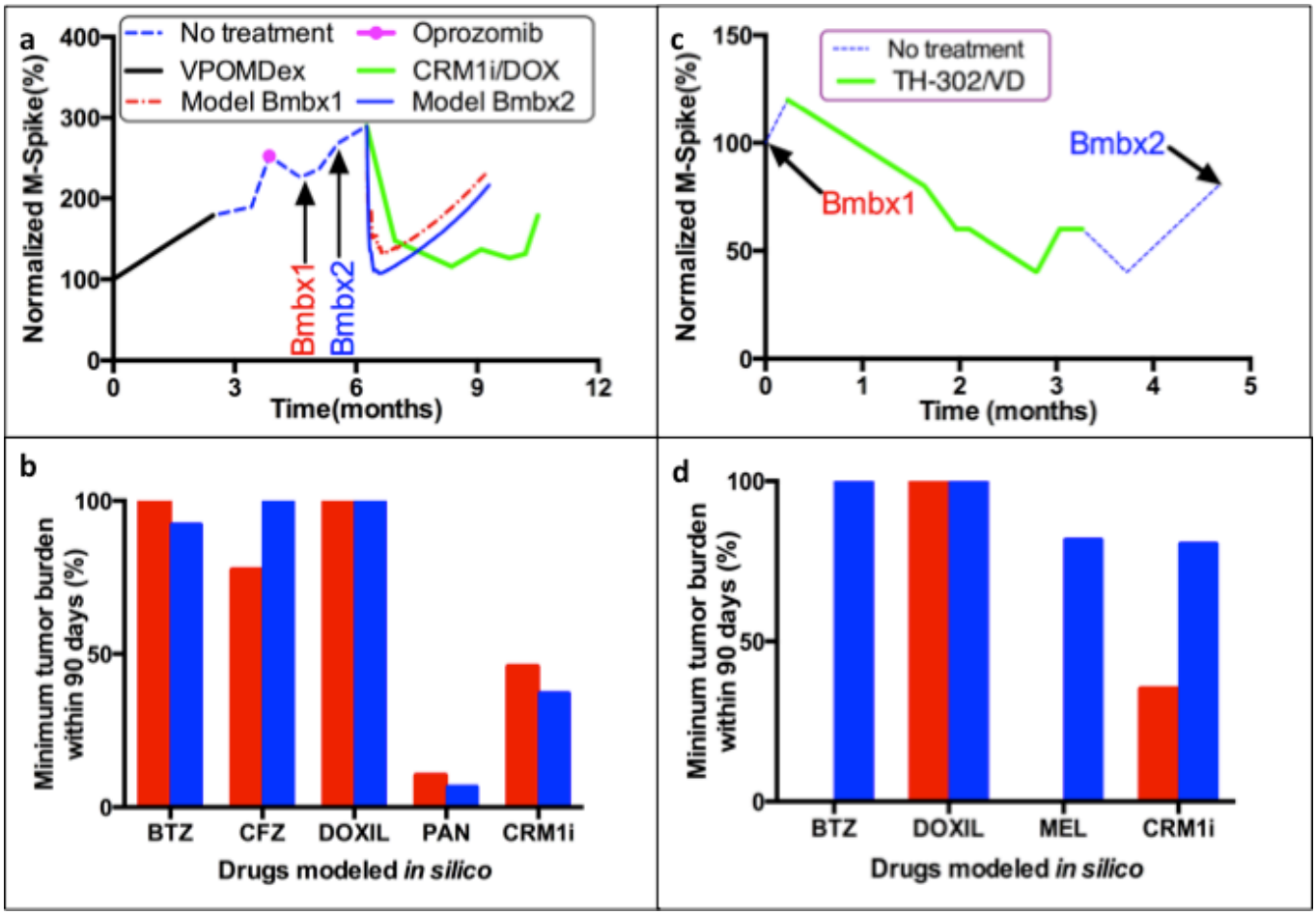


**Supplemental Figure 13.** ***Ex vivo*** **chemosensitivity in sequential biopsies in absence and during treatment.** (**a**) To assess the inter-day reproducibility of the *ex vivo* assay (test-retest) we have quantified the chemosensitivity of one patient (**Pt52**) with two biopsies separated by one month without treatment and used this information to build mathematical models of predicted clinical response to therapy (CRM1i) using the *ex vivo* data from both biopsies (red dashed line for biopsy 1, blue solid line for biopsy 2), indicating high correlation between both modeled curves (Pearson r=0.9707) and thus reproducibility of assay. (**b**) Variation of mathematical model clinical predictions of best response built with *ex vivo* data from two sequential biopsies (**Pt52**). (**c**) Two biopsies of patient **Pt32**, separated by treatment with Th-302, bortezomib and dexamethasone, were tested for *ex vivo* chemosensitivity (this patient had the dose of bortezomib reduced from 1.3mg/m$^2$ to 1mg/m$^2$ due to thrombocytopenia). (**d**) Model predictions indicate that the patient, who was initially sensitive to proteasome inhibitors and alkylating agents, has become refractory to both.

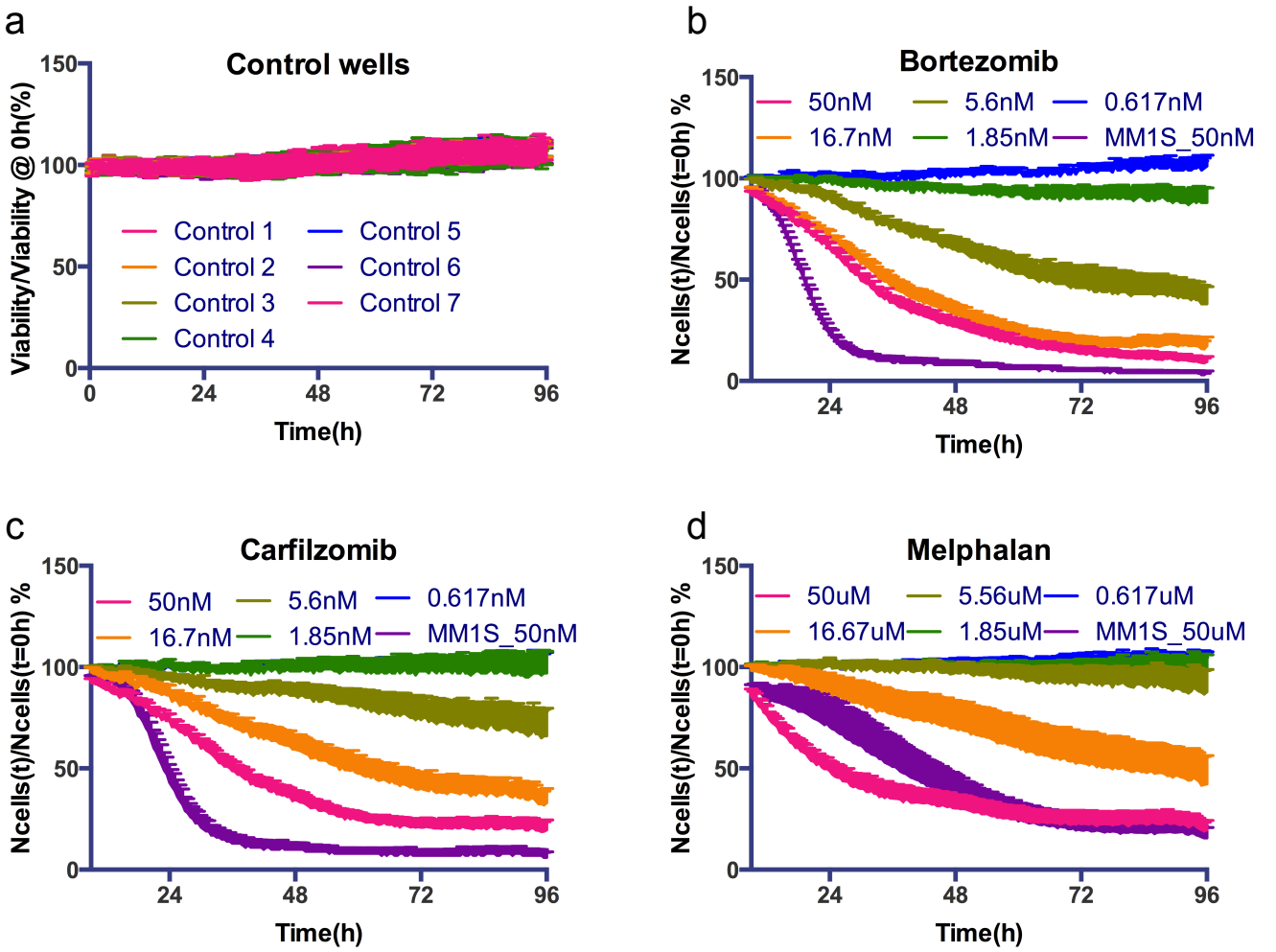


**Supplemental Figure 14. Intra-plate variation of *ex vivo* assay.** Primary cells from a patient (Pt48) were seeded as usual in a 384-well plate and tested in a pattern of three different drugs (bortezomib, melphalan and carfilzomib), at five concentrations and two replicates, and a negative control (no drugs added). This pattern was repeated 8 times across the plate and standard deviation (S.D.) of dose response curves for each drug and concentration were determined. Maximum S.D. values were 3.4% for melphalan, 6.3% for bortezomib, 8.9% for carfilzomib, and 6.7% for controls.

## 1 Population – No Distribution

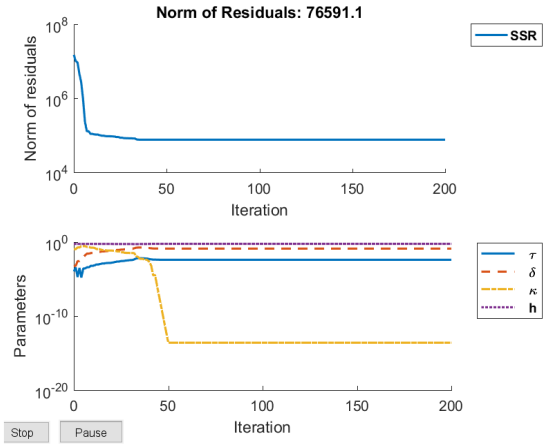


## 2 Populations – No Distribution

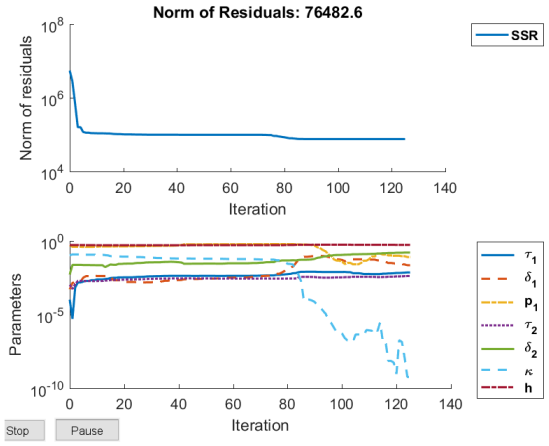


## 1 Population – Distribution

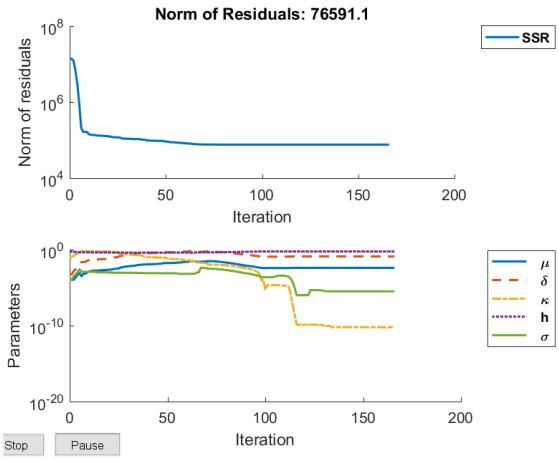


## 2 Populations – Distribution

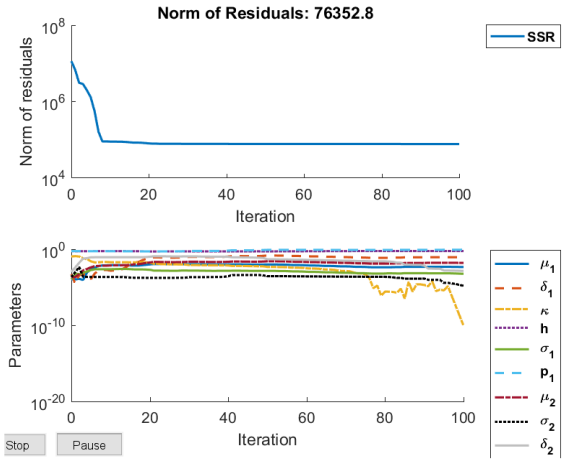


**Supplemental Figure 15. Convergence study comparing the four population models for panobinostat.**

| | 1 Pop – No Dist. | 2 Pops – No Dist. | 1 Pop – Dist. | 2 Pops – Dist. |
|---|---|---|---|---|
| Sum of Squares of Residuals (SSR) | 76,591.1 | 76,482.6 | 76,591.1 | 76,352.8 |
| Number of parameters (k) | 4 | 7 | 5 | 9 |
| Akaike Information Criterion (AIC) | 76.2234 | 76.2533 | 76.2434 | 76.2572 |

**Supplemental Table 4. SSR, number of parameters, and AIC values for the four models for patient Pt103's *ex vivo* sensitivity to panobinostat.**

## 1 Population - No Distribution

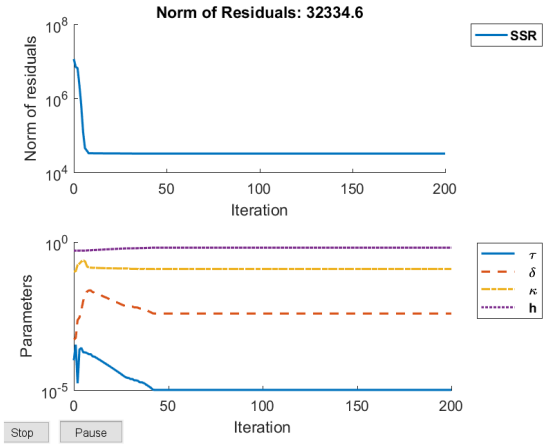


## 2 Populations - No Distribution

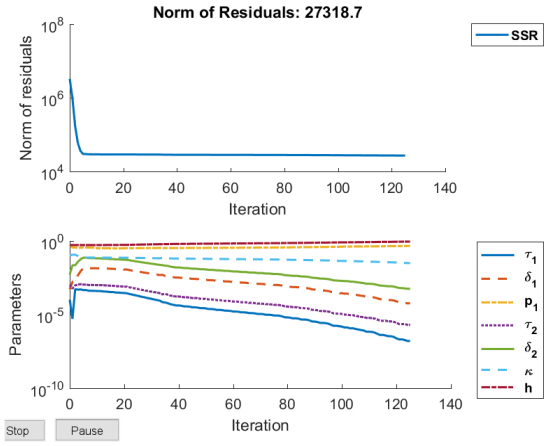


## 1 Population - Distribution

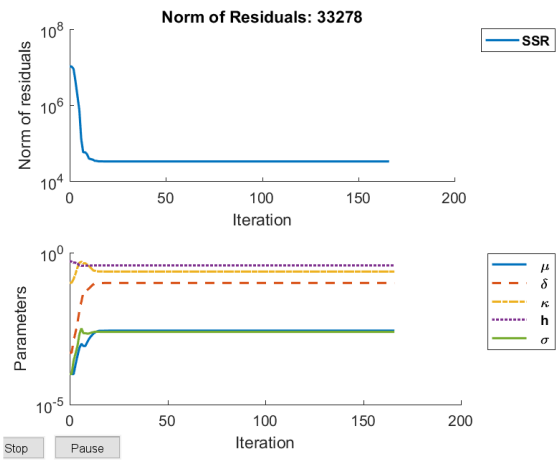


## 2 Populations – Distribution

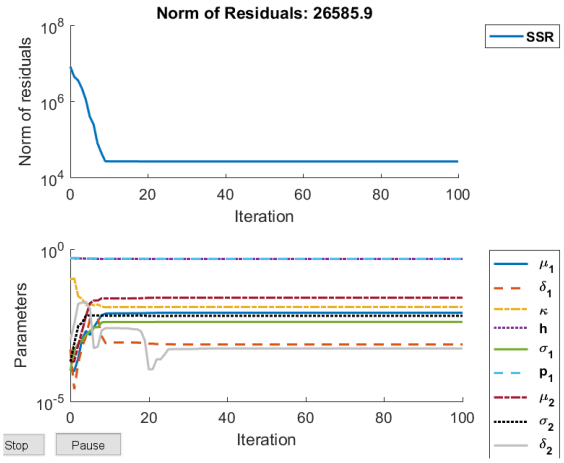


**Supplemental Figure 16. Convergence study comparing the four population models for carfilzomib.**

| | 1 Pop – No Dist. | 2 Pops – No Dist. | 1 Pop – Dist. | 2 Pops – Dist. |
|---|---|---|---|---|
| Sum of Squares of Residuals (SSR) | 32,334.6 | 27,318.7 | 33,278.0 | 26,585.9 |
| Number of parameters (k) | 4 | 7 | 5 | 9 |
| Akaike Information Criterion (AIC) | 57.9158 | 54.3972 | 58.5464 | 53.8599 |

**Supplemental Table 5. SSR, number of parameters, and AIC values for the four models for carfilzomib.**

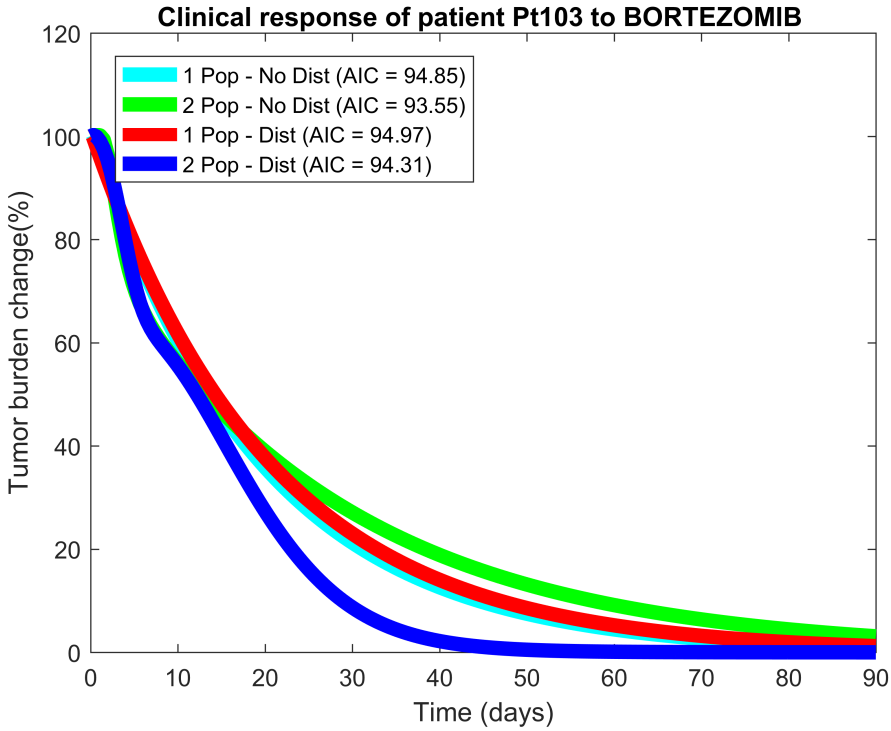


**Supplemental Figure 17. Comparison between clinical predictions for bortezomib using the four models.**

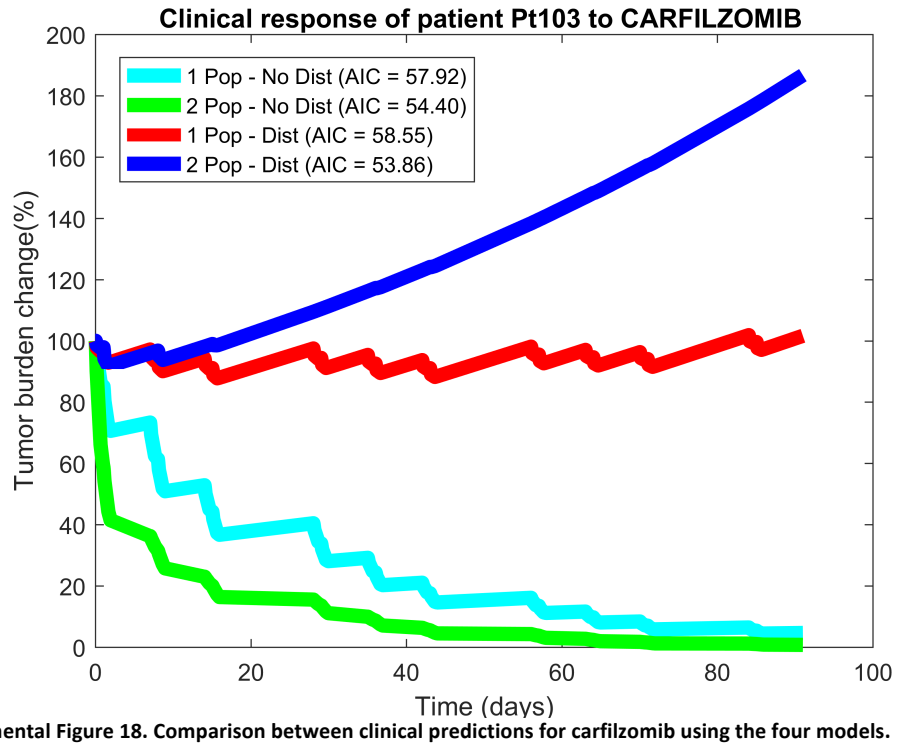


**Supplemental Figure 18. Comparison between clinical predictions for carfilzomib using the four models.**

**Data Processing Guide:**

The flow of data analysis consists in multiple steps: (a) running the digital image analysis algorithm in imageJ; (b) creation of a description file assigning each well in the plate to a particular drug and concentration; (c) grouping the results from image analysis of wells according to drugs and concentrations, normalizing results by control and time 0h; (d) creation of charts in Prism Graphpad format; and (e) generation of Matlab code for analysis of chemosensitivity as well as estimates of clinical response. These steps are automated by different pieces of software developed in Javascript (for ImageJ), Java and Matlab, and are provided below.

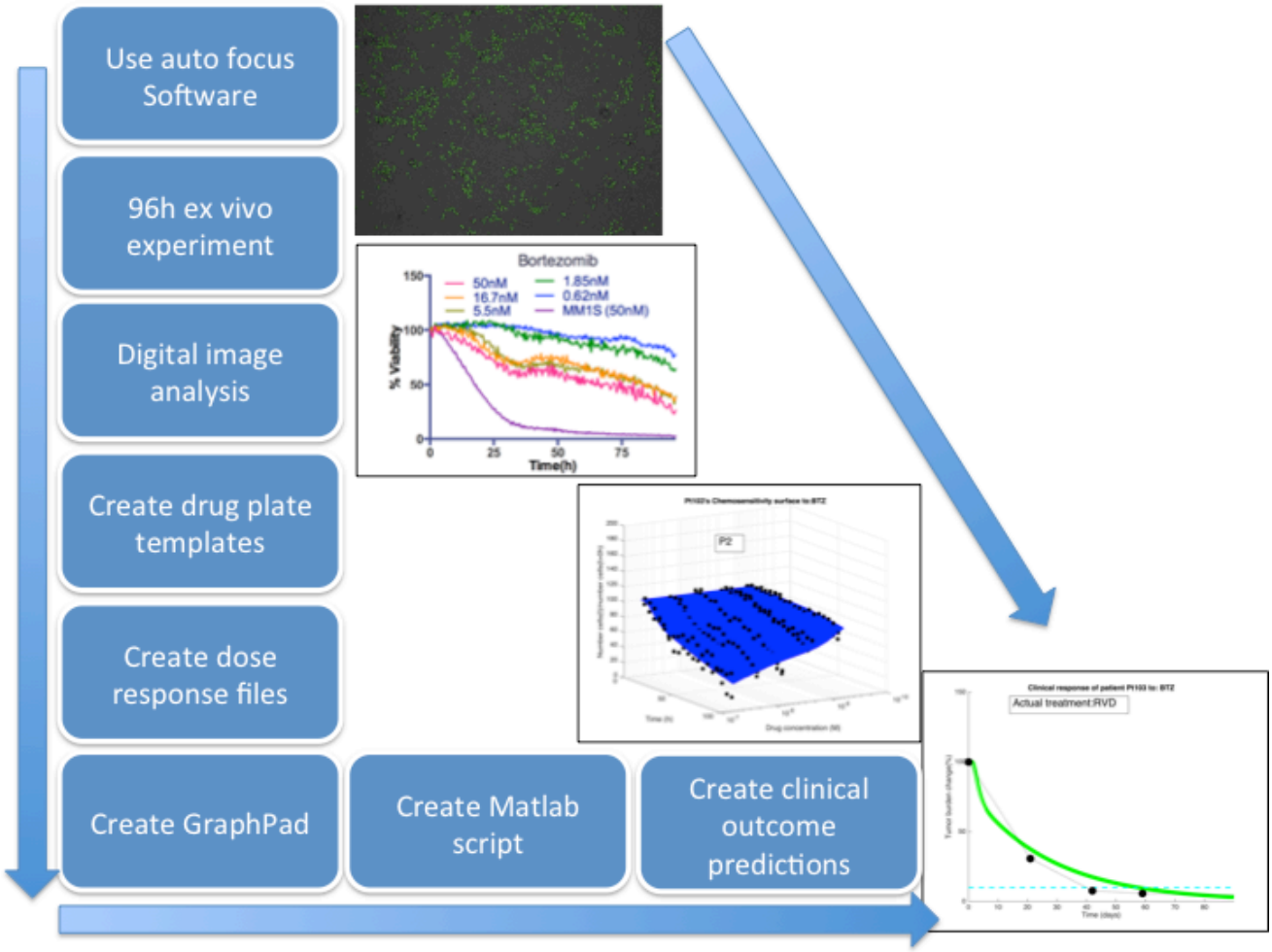

# Use auto focus software

- Open template file with pre-defined beacons;
- Set beacons 1, 24, 180, 181, 361 and 384;
- Run time lapse and stop after at least one beacon was imaged;
- Save results;
- Open template file using software CalibrateFocus.jar (below, arrow 1)

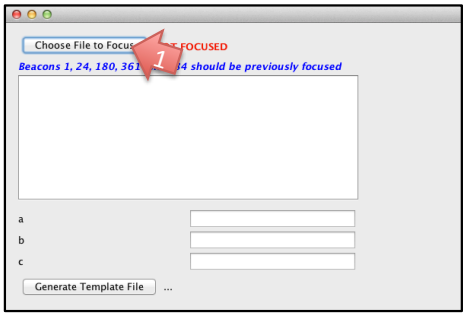


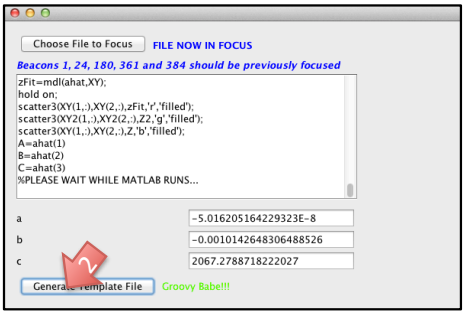


- One the file is read, the software will calculate the correct focal “plane”;
- Press the “Generate template file” and close the software;
- Re-open the now focused template file in and run the time lapse;

# Digital image analysis

- Copy the folder containing all beacons into cluster's "parent folder";
- Open the file BatchGenerator.sh and change the value of the property "folder" to the name of the folder containing all the beacons;
- Open the file BatchStart.txt and edit the path imageJ, imageJ script and "parent folder" where the folder with beacons are stored:
  - Default imageJ path: /home/silvaa/fiji
  - Default imageJ macro path: /home/silvaa/fiji/macros/MacroAnalysis384_14Cluster.ijm
  - Default "parent folder" containing all beacons: /share/data/evos_silva**/$folder/Beacon-$beacon**
- **Do not replace the text in red.**
- Run the analysis with the command line: bash ./BatchGenerator.sh
- Once the jobs are completed, a folder named "tiffs" will be created inside the "folder" directory. Inside "tiffs" there will be a video for each beacon as well as a results.csv file with the time lapse analysis of all beacons;

# Create drug plate templates

- Open the template file DrugList.csv;
- Edit the names of drugs in the file according to their spatial location in the drug plate used in the robotic plate handler;
- Modify the maximum concentration (final) for each drug. For instance, if the maximum concentration in the 384-well plate with cells is 10uM, then enter this value here;
- Run the software BuildExperimentalDesign.jar and pass as parameter the path to the folder containing the Druglist.csv file. For instance:
  - java -cp BuildExperimentalDesign.jar BuildExperimentalDesign "/Users/silvaa/Desktop/Pt in cluster/Pt101"
- The software creates two folders named "PtSample" and "MM1_S". The first contains the list of beacons and corresponding drug names and concentrations for the wells with primary cells, and the second for the cell line positive control. Each folder has a unique file name ExperimentalDesign.txt;

# Create dose response files

- Copy the file “results.csv” inside both “PtSample” and “MM1_S” folders;
- Run software Evos384.jar;

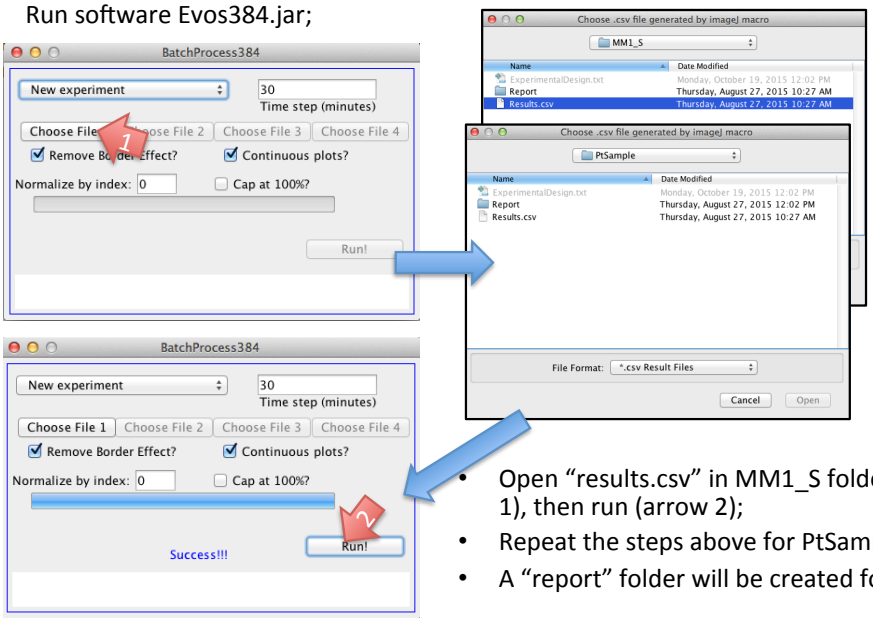


- Open “results.csv” in MM1_S folder (arrow 1), then run (arrow 2);
- Repeat the steps above for PtSample;
- A “report” folder will be created for each;

# Create GraphPad

- Run the software to build the GraphPad report and It will generate a file named Report.pzfx:
  - java -cp BuildGraphPadFile.jar BuildGraphPadFile "/Users/silvaa/Desktop/Pt in cluster/Pt101”
- Open the file using GraphPad and ignore the error message;
- Open the leaflet “info” and delete one of the two “Project info 1” items;
- Save the file with an alternative name, e.g. ReportPt101.pzfx;
- Re-open the file and there should be no error messages;
- Each of the 31 drugs and control should be depicted in a separate chart and numeric values in data tables;
- All values are normalized by negative controls and are 100% at timepoint 0h.

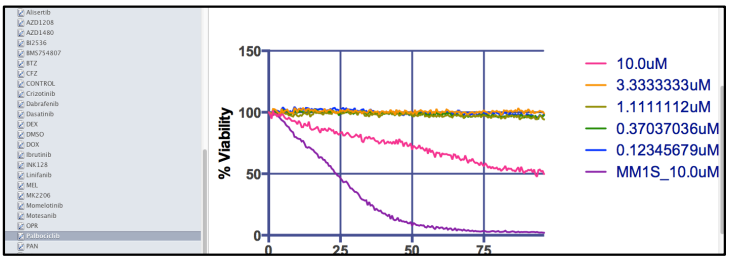

# Create Matlab script

- Run the software to build Matlab code for clinical predictions based on patient ex vivo results:
  - java -cp GenerateMatlabGraphFormat.jar GenerateMatlabGraphFormat "/Users/silvaa/Desktop/Pt in cluster/PtPathList.txt"
  - The file PtPathList.txt contains the folder where the Matlab script files will be stored (1) as well as the folders where each patient ex vivo results are stored (2). The syntax is: path to patient folder where ex vivo results are stored;-1;1;,;number of hours of experiment;patient identifier

```
/Users/silvaa/Desktop/Career/Manuscripts 2014/ModelingPredictionTherapyRes[illegible]e/Nature Medicine/Drug Synergy
/Users/silvaa/Desktop/Pt in cluster/Pt6/Report;-1;1;,;96;Pt6
/Users/silvaa/Desktop/Pt in cluster/Pt7/Report;-1;1;,;72;Pt7
/Users/silvaa/Desktop/Pt in cluster/Pt9/Report;-1;1;,;72;Pt9
/Users/silvaa/Desktop/Pt in cluster/Pt10+11/Pt10/Report;-1;1;,;90;Pt10
/Users/silvaa/Desktop/Pt in cluster/Pt10+11/Pt11/LenAsControl/Report;-1;1;,;90;Pt11
```

- The output will be the number of patients analyzed as well as any errors found:

```
Running.....Finished processing 57 patients.
```

- A file with each patient's ID will be created. To run the analysis, copy and paste code into Matlab

# Create clinical outcome predictions

- Run the software that creates a single Matlab script file for ex vivo, drug combination synergy and clinical outcome predictions for all patients:
  - java -cp DrugListSynergy.jar DrugListSynergy "/Users/silvaa/Desktop/Career/Manuscripts 2014/ModelingPredictionTherapyResponse/Nature Medicine/Drug Synergy"
  - Where the folder above contains the file DrugListSynergy.txt with the list of drugs and combinations to be modeled. Add new drugs to the bottom of the list.
  - A file named RunAllPatients.m will be generated. Copy this file to Matlab path and run the command RunAllPatients in Matlab's command line. Figures (.fig and .png) will be created in the folder */matlabFiles*:
    - Ptxx_DrugY_Clinical_Prediction: the treatmet simulation if there is an available PK model for the drug;
    - Ptxx_ClinicalRadar: bar plot with the minimum tumor, normalized by day 0, within an interval of 90 days, for the simulated drug as single agent;
    - Ptxx_ExVivo_DrugY: the ex vivo chemosensitivity dose response and fitting models;
    - Ptxx_ExVivoRadar: bar plot with AUC (area under curve) of dose response surfaces for the duration of the experiment;
    - Ptxx_LD50Radar: bar plot with LD50 concentrations (in molar) for the last time point of the experiment (default 96h);
    - Ptxx_Drug1+Drug2_Synergy: heatmaps comparing efficacy of drug combination versus either drug as single agent as well as conditions of synergy;

**Supplemental References:**


1. Winter, G.E.*, et al.* Systems-pharmacology dissection of a drug synergy in imatinib-resistant CML. *Nat Chem Biol* **8**, 905-912 (2012).
2. Hideshima, T., Richardson, P.G. & Anderson, K.C. Mechanism of action of proteasome inhibitors and deacetylase inhibitors and the biological basis of synergy in multiple myeloma. *Mol Cancer Ther* **10**, 2034-2042 (2011).
3. Turner, J.G.*, et al.* CRM1 Inhibition Sensitizes Drug Resistant Human Myeloma Cells to Topoisomerase II and Proteasome Inhibitors both In Vitro and Ex Vivo. *J Cancer* **4**, 614-625 (2013).
4. Chou, T.C. Drug combination studies and their synergy quantification using the Chou-Talalay method. *Cancer Res* **70**, 440-446 (2010).
5. Greco, W.R., Faessel, H. & Levasseur, L. The search for cytotoxic synergy between anticancer agents: a case of Dorothy and the ruby slippers? *J Natl Cancer Inst* **88**, 699-700 (1996).
6. Shargel, L., Wu-Pong, S. & Yu, A.B.C. *Applied biopharmaceutics & pharmacokinetics*, (Appleton & Lange Reviews/McGraw-Hill, Medical Pub. Division, New York, 2005).
7. Clark, A.J. The reaction between acetyl choline and muscle cells. Part II. *J Physiol-London* **64**, 123-143 (1927).
8. Akaike, H. New Look at Statistical-Model Identification. *Ieee T Automat Contr* **Ac19**, 716-723 (1974).
9. Jelinek, T. & Hajek, R. Monoclonal antibodies - A new era in the treatment of multiple myeloma. *Blood Rev* **30**, 101-110 (2016).
10. Lokhorst, H.M.*, et al.* Targeting CD38 with Daratumumab Monotherapy in Multiple Myeloma. *N Engl J Med* **373**, 1207-1219 (2015).